Available online at www.sciencedirect.com
SCIENCE DIRECT®
Journal of Sound and Vibration 293 (2006) 227–252
JOURNAL OF SOUND AND VIBRATION
www.elsevier.com/locate/jsvi

# Dynamic instability and chaos of empty and fluid-filled circular cylindrical shells under periodic axial loads

F. Pellicano[a,*], M. Amabili[b]

[a]Dipartimento di Ingegneria Meccanica e Civile, Università di Modena e Reggio Emilia, V. Vignolese, 905, Modena I-41100, Italy
[b]Dipartimento di Ingegneria Industriale, Università di Parma, Parco Area delle Scienze, 181/A, Parma, I-43100, Italy

Received 28 February 2005; received in revised form 30 August 2005; accepted 29 September 2005
Available online 10 January 2006

**Abstract**

In the present paper the dynamic stability of circular cylindrical shells subjected to static and dynamic axial loads is investigated. Both Donnell's nonlinear shallow shell and Sanders–Koiter shell theories have been applied to model finite-amplitude static and dynamic deformations. Results are compared in order to evaluate the accuracy of these theories in predicting instability onset and post-critical nonlinear response. The effect of a contained fluid on the stability and the post-critical behaviour is analyzed in detail. Geometric imperfections are considered and their influence on the dynamic instability and post-critical behaviour is investigated. Chaotic dynamics of pre-compressed shells is investigated by means of nonlinear time-series techniques, extracting correlation dimension and Lyapunov exponents.


## 1. Introduction

The stability of shells has been deeply investigated in the past. In fact, these structural elements play an important role in many fields, such as: nuclear, aerospace, civil and mechanical engineering. The complexity in finding accurate models useful for practical designers, gave rise to an enormous scientific production, focused in particular on static buckling. Nevertheless, many authors consider that the general problem of shell stability is still open.

An interesting review on shell stability is due to Babcock [1]. After a certain criticism about the number of papers published on the subject, about 50,000!, he focused the attention on the most important topics on this field: post-buckling and imperfection sensitivity; dynamic buckling; plastic buckling; experiments. It is now clear that the most important types of imperfections are the geometrical ones; unfortunately, it is not simple to relate them to the knockdown factor. The most of the literature cited in Ref. [1] about dynamic buckling is concerned with dynamic step-loading, i.e. transient analyses.

Calladine [2], in his review on imperfection sensitivity, confirmed that the buckling of thin-walled shells has been still "imperfectly" understood; however, he claimed that "there are strong grounds for supposing that locked-in initial stresses on account of imperfect initial geometry and the static indeterminacy of boundary conditions of real shells have a pronounced effect on the buckling performance". He showed several

*Corresponding author. Tel.: +39 059 2056154; fax: +39 059 2056129.
*E-mail addresses:* francesco.pellicano@unimore.it (F. Pellicano), marco@me.unipr.it (M. Amabili).

0022-460X/$ - see front matter © 2005 Elsevier Ltd. All rights reserved.
doi:10.1016/j.jsv.2005.09.032

interesting approximate formulas for actual buckling prediction; he discussed the problem of coincident buckling modes and concluded that a great attention should be addressed to initial geometric imperfections as well as to locked-in stresses, due for example to fixed boundaries.

In a more recent review on shell's buckling [3], the previous considerations were confirmed, i.e. the field of shell's stability still presents several problems to be investigated.

Even though the stability of shells subjected to axial periodic loads received less attention with respect to the static buckling, the literature is rich of interesting papers; many of them are from Eastern Europe or former Soviet Union, as shown in the extensive review by Amabili and Païdoussis on nonlinear vibrations and dynamics of shells [4].

One of the first studies on parametric instability of cylindrical shells is due to Yao [5], who reduced parametric oscillations (by using Donnell's nonlinear shallow shell theory, axial dynamic loads do not give direct excitation to the equation of motion but their contribution appears as parametric excitation) of circular cylindrical shells to the well-known Mathieu equation, and studied the stability bounds. Vijayaragham and Evan-Iwanowski [6] studied theoretically and experimentally the dynamic instability of clamped-free seismically excited cylindrical shells.

An interesting experimental study on parametric resonances of cylindrical shells can be found in Ref. [7], where the author observed a particularly violent instability; it takes place suddenly (the authors defined it a "bang") when a transition between stable to unstable regions occurs (or between two different instability regions involving different modes). Unfortunately, authors did not explain the nature of such "bang" that often damaged the shell.

Donnell's nonlinear shallow shell equations were used in Ref. [8] to study parametric oscillations of circular cylindrical shells. In that paper it was pointed out that: using membrane approximation, to evaluate in-plane stresses, can lead to large errors when axisymmetric modes are close to the resonance.

Kubenko and Koval'chuk [9] published an interesting review on nonlinear problems of shells, where interesting results were reported about parametric vibrations and in particular: type of nonlinearity; imperfections, experiments, damping models. They in particular pointed out the limitation of analytical studies concerning with reduced order models.

Pellicano et al. [10] studied nonlinear oscillations and dynamical instability of simply supported cylindrical shells, under the action of longitudinal dynamic force, with fluid–structure interaction; Donnell's nonlinear shallow shell theory was applied and a multimode approach was developed.

Gonçalves and Del Prado [11] analyzed the dynamic buckling of a perfect circular cylindrical shell under axial static and dynamic loads. Donnell's nonlinear shallow shell theory was used and the membrane theory was considered to evaluate the in-plane stresses. The partial differential operator was discretized through the Galerkin technique, using a relatively large modal expansion. However, no companion mode participation was considered and the boundary conditions were dropped by assuming an infinitely long shell. Escape from potential well was analyzed in detail, and a correlation of this phenomenon with the parametric resonance was given. Popov [12] used a continuation technique to study nonlinear oscillations and parametric instabilities of an infinitely long cylindrical shell.

An analytical simplified approach was developed by Jansen [13] in order to simulate dynamic step and periodic axial loads acting on isotropic and anisotropic shells, showing that simple periodic responses can be simulated through low dimensional models. The effect of in-plane inertia was included in the Donnell-type equations used in such a paper: it was found that neglecting in-plane inertia gives rise to a moderate underestimate of the instability region.

In Ref. [14] a multimode approach was developed to analyze the correlation of parametric instability with shell collapse, considering the geometric imperfections.

In the present paper, dynamic instability and post-critical response of circular cylindrical shells under the action of axial static and periodic forces are investigated. Geometric imperfections and the presence of a contained liquid are considered.

Sanders–Koiter and Donnell's nonlinear shallow shell theories are used for structural modelling; potential flow theory is applied for fluid–structure interaction. Multi-mode expansions of the displacement fields of the shell are developed. Lagrange equations (for the Sanders–Koiter theory) and Galerkin (for the Donnell's nonlinear shallow shell theory) approach are applied in order to reduce partial differential equations (PDE) to

ordinary differential equations (ODE). Convergence tests are carried out in order to assure a suitable accuracy of the results. Comparisons between the two shell theories are performed in order to evaluate the accuracy of the Donnell's nonlinear shallow shell theory. The effect of imperfections and the presence of fluid on the dynamic behaviour of the shell are numerically investigated; in particular, the effect on the instability onset is studied.

In order to obtain a complete dynamic scenario, numerical analyses are carried out by means of continuation techniques (AUTO 97 [15]) and direct simulations, obtaining: static and periodic responses with stability analysis and bifurcations; bifurcation diagrams; Poincaré maps; time histories; frequency spectra.

By taking advantage of nonlinear time series techniques [16], Lyapunov exponents, Kaplan–Yorke and Correlation dimensions have been evaluated from direct simulation, in order to reach a deep understanding of the complex dynamics.

## 2. Equations of motion and discretization: Sanders–Koiter theory

In order to take advantage from the axial symmetry of circular cylindrical shells a cylindrical coordinate system ($O$; $x$, $r$, $\theta$), Fig. 1, is considered. The origin $O$ is located at the centre of one end of the shell. The in-plane and radial displacement fields of the middle shell surface are denoted by $u(x, \theta, t)$, $v(x, \theta, t)$ and $w(x, \theta, t)$, in the axial, circumferential and radial directions, respectively; $w$ is taken positive outwards.

Radial initial imperfections, given by the displacement field $w_0(x, \theta)$, are considered.

### 2.1. Sanders–Koiter theory: strain energy

The Sanders–Koiter theory is based on Love's first approximation: (i) $h \ll R$, where $h$ and $R$ are the shell thickness and radius, respectively; (ii) strains are small; (iii) transverse normal stress is small; and (iv) the normal to the undeformed middle surface remains straight and normal to the middle surface after deformation and undergoes no thickness stretching (Kirchhoff–Love kinematic hypothesis) [17,18]; (v) rotary inertia and shear deformations are neglected. Strain components $\varepsilon_x$, $\varepsilon_\theta$ and $\gamma_{x\theta}$ at an arbitrary point of the shell are related to the middle surface strains $\varepsilon_{x,0}$, $\varepsilon_{\theta,0}$ and $\gamma_{x\theta,0}$ and to the changes in the curvature and torsion of the middle surface $k_x$, $k_\theta$ and $k_{x\theta}$ by the following three relationships [17]

$$\varepsilon_x = \varepsilon_{x,0} + zk_x, \tag{1a}$$

$$\varepsilon_\theta = \varepsilon_{\theta,0} + zk_\theta, \tag{1b}$$

$$\gamma_{x\theta} = \gamma_{x\theta,0} + zk_{x\theta}, \tag{1c}$$

where $z$ is the distance of the arbitrary point of the shell from the middle surface (see Fig. 1(b)).

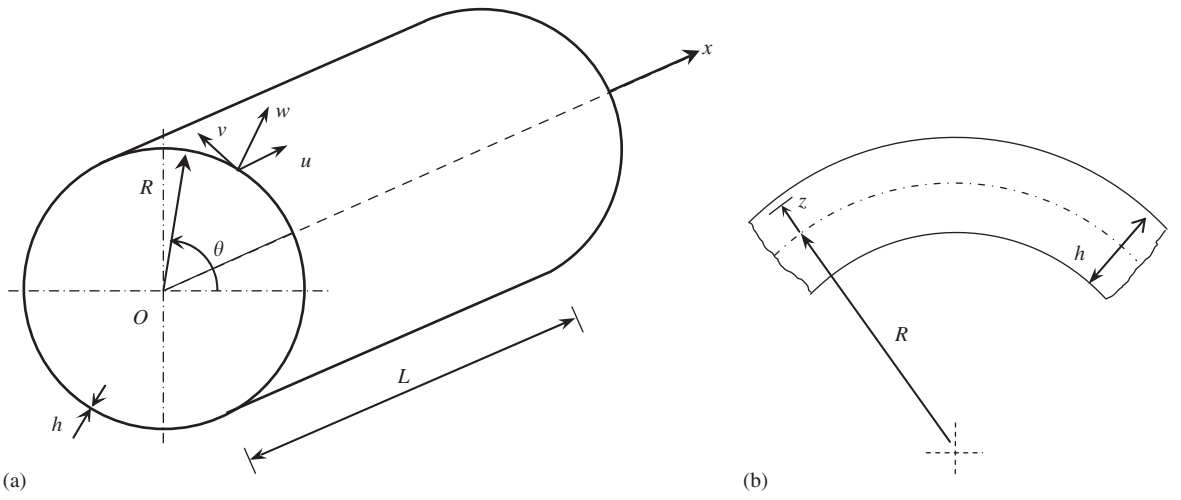


Fig. 1. Circular cylindrical shell: coordinate system and dimensions. (a) Complete shell; (b) cross-section of the shell surface.

According to the Sanders–Koiter theory, the middle surface strain–displacement relationships, changes in the curvature and torsion are given by [17]

$$\varepsilon_{x,0} = \frac{\partial u}{\partial x} + \frac{1}{2}\left(\frac{\partial w}{\partial x}\right)^2 + \frac{1}{8}\left(\frac{\partial v}{\partial x} - \frac{\partial u}{R\partial\theta}\right)^2 + \frac{\partial w}{\partial x}\frac{\partial w_0}{\partial x}, \tag{2a}$$

$$\varepsilon_{\theta,0} = \frac{\partial v}{R\partial\theta} + \frac{w}{R} + \frac{1}{2}\left(\frac{\partial w}{R\partial\theta} - \frac{v}{R}\right)^2 + \frac{1}{8}\left(\frac{\partial u}{R\partial\theta} - \frac{\partial v}{\partial x}\right)^2 + \frac{\partial w_0}{R\partial\theta}\left(\frac{\partial w}{R\partial\theta} - \frac{v}{R}\right), \tag{2b}$$

$$\gamma_{x\theta,0} = \frac{\partial u}{R\partial\theta} + \frac{\partial v}{\partial x} + \frac{\partial w}{\partial x}\left(\frac{\partial w}{R\partial\theta} - \frac{v}{R}\right) + \frac{\partial w_0}{\partial x}\left(\frac{\partial w}{R\partial\theta} - \frac{v}{R}\right) + \frac{\partial w}{\partial x}\frac{\partial w_0}{R\partial\theta}, \tag{2c}$$

$$k_x = -\frac{\partial^2 w}{\partial x^2}, \tag{2d}$$

$$k_\theta = \frac{\partial v}{R^2\partial\theta} - \frac{\partial^2 w}{R^2\partial\theta^2}, \tag{2e}$$

$$k_{x\theta} = -2\frac{\partial^2 w}{R\partial x\partial\theta} + \frac{1}{2R}\left(3\frac{\partial v}{\partial x} - \frac{\partial u}{R\partial\theta}\right). \tag{2f}$$

The elastic strain energy $U_S$ of a circular cylindrical shell, neglecting $\sigma_z$ as stated by Love's first approximation, is given by [18]

$$U_S = \frac{1}{2}\int_0^{2\pi}\int_0^L\int_{-h/2}^{h/2}\left(\sigma_x\,\varepsilon_x + \sigma_\theta\,\varepsilon_\theta + \tau_{x\theta}\,\gamma_{x\theta}\right)\mathrm{d}x\,R\,(1 + z/R)\,\mathrm{d}\theta\,\mathrm{d}z, \tag{3}$$

where $L$ is the shell length and the stresses $\sigma_x$, $\sigma_\theta$ and $\tau_{x\theta}$ are related to the strain for homogeneous and isotropic material ($\sigma_z = 0$, case of plane stress) by [18]

$$\sigma_x = \frac{E}{1-\nu^2}(\varepsilon_x + \nu\varepsilon_\theta), \tag{4a}$$

$$\sigma_\theta = \frac{E}{1-\nu^2}(\varepsilon_\theta + \nu\varepsilon_x), \tag{4b}$$

$$\tau_{x\theta} = \frac{E}{2(1+\nu)}\gamma_{x\theta}, \tag{4c}$$

where $E$ is the Young modulus and $\nu$ is the Poisson ratio.

Using Eqs. (1,3,4), the following expression is obtained

$$\begin{aligned} U_S = {} & \frac{1}{2}\frac{Eh}{1-\nu^2}\int_0^{2\pi}\int_0^L\left(\varepsilon_{x,0}^2 + \varepsilon_{\theta,0}^2 + 2\nu\varepsilon_{x,0}\varepsilon_{\theta,0} + \frac{1-\nu}{2}\gamma_{x\theta,0}^2\right)\mathrm{d}x R\,\mathrm{d}\theta \\ & + \frac{1}{2}\frac{Eh^3}{12(1-\nu^2)}\int_0^{2\pi}\int_0^L\left(k_x^2 + k_\theta^2 + 2\nu k_x k_\theta + \frac{1-\nu}{2}k_{x\theta}^2\right)\mathrm{d}x R\,\mathrm{d}\theta + O(h^4), \end{aligned} \tag{5}$$

where $O(h^4)$ is a higher-order term in $h$ according to the Sanders–Koiter theories.

In Eq. (5), the first term is the membrane (also referred to as stretching) energy and the second one is the bending energy.

The kinetic energy $T_S$ of a circular cylindrical shell (rotary inertia is neglected) is given by

$$T_S = \frac{1}{2}\rho_S h\int_0^{2\pi}\int_0^L(\dot{u}^2 + \dot{v}^2 + \dot{w}^2)\,\mathrm{d}x R\,\mathrm{d}\theta, \tag{6}$$

where $\rho_S$ is the mass density of the shell. In Eq. (6) the overdot denotes a time derivative.

The virtual work $W$ done by the external forces is written as

$$W = \int_0^{2\pi} \int_0^L (q_x u + q_\theta v + q_r w)\, \mathrm{d}x\, R\, \mathrm{d}\theta, \tag{7}$$

where $q_x$, $q_\theta$ and $q_r$ are the distributed forces per unit area acting in axial, circumferential and radial directions, respectively.

The following boundary conditions are imposed at the shell ends, $x = 0$, $L$:

$$w = w_0 = 0, \tag{8a}$$

$$M_x = 0, \tag{8b}$$

$$\partial^2 w_0/\partial x^2 = 0, \tag{8c}$$

$$N_x = \frac{\tilde{P}}{2\pi R}, \tag{8d}$$

$$v = 0, \tag{8e}$$

where $M_x$ is the bending moment per unit length and $N_x$ is the axial force per unit length, $\tilde{P}$ is the external axial load; moreover, $u$, $v$ and $w$ must be continuous in $\theta$.

Note that the boundary condition (8d) will be relaxed and substituted with $N_x = 0$ in the following; because the effect of axial loads will be included in the Lagrangian equations by means of their virtual work. Therefore, boundary conditions for a classical simply supported shell are assumed.

### 2.2. Sanders–Koiter theory: modal expansion

In order to reduce the system to finite dimensions, i.e. to transform the initial PDE system into a set of ODE, the middle surface displacements $u$, $v$ and $w$ are expanded by using trial functions. In the present work $u$, $v$ and $w$ are expanded by using the eigenmodes of the simply supported, empty shell (which are unchanged for the completely filled shell with open ends). In the past this kind of expansion showed good convergence properties when the linear modes are carefully chosen: one has to select all modes that can undergo to a linear, parametric or nonlinear resonance, then further modes driven by the nonlinear coupling should be added up to convergence.

The expansion used in the present work is the following:

$$u(x,\theta,t) = \sum_{m=1}^{M_{u,1}} \sum_{j=1}^{N_u} [u_{m,j,c}(t)\cos(\mathrm{j}\theta) + u_{m,j,s}(t)\sin(\mathrm{j}\theta)]\cos(\lambda_m x) + \sum_{m=1}^{M_{u,2}} u_{m,0}(t)\cos(\lambda_m x), \tag{9a}$$

$$v(x,\theta,t) = \sum_{m=1}^{M_{v,1}} \sum_{j=1}^{N_v} [v_{m,j,c}(t)\sin(\mathrm{j}\theta) + v_{m,j,s}(t)\cos(\mathrm{j}\theta)]\sin(\lambda_m x) + \sum_{m=1}^{M_{v,2}} v_{m,0}(t)\sin(\lambda_m x), \tag{9b}$$

$$w(x,\theta,t) = \sum_{m=1}^{M_{w,1}} \sum_{j=1}^{N_w} [w_{m,j,c}(t)\cos(\mathrm{j}\theta) + w_{m,j,s}(t)\sin(\mathrm{j}\theta)]\sin(\lambda_m x) + \sum_{m=1}^{M_{w,2}} w_{m,0}(t)\sin(\lambda_m x), \tag{9c}$$

where j is the number of circumferential waves, $m$ is the number of longitudinal half-waves, $\lambda_m = m\pi/L$ and $t$ is the time; $u_{m,j}(t)$, $v_{m,j}(t)$ and $w_{m,j}(t)$ are the generalized coordinates that are unknown functions of $t$; the additional subscript $c$ or $s$ indicates if the generalized coordinate is associated to symmetric and anti-symmetric mode shapes in $\theta$ (no additional subscript is used for axisymmetric terms). The integers $N_u$, $N_v$, $N_w$, $M_{u,1}$, $M_{u,2}$, $M_{v,1}$, $M_{v,2}$, $M_{w,1}$ and $M_{w,2}$ must be selected with care in order to obtain the required accuracy and acceptable dimension of the nonlinear problem.

The excitation will be set in the neighbourhood of principal parametric resonance of mode with $m = 1$ longitudinal half-wave and $n$ circumferential waves, indicated as resonant mode ($m$, $n$) for simplicity. It is

observed, for symmetry reasons, that the nonlinear interaction among linear modes of the chosen basis includes: asymmetric modes ($n>0$) having a given $n$ value (e.g. the resonant mode), asymmetric modes having a multiple of this value of circumferential waves ($k\times n$, where $k$ is an integer), and axisymmetric modes ($n=0$); asymmetric modes with different numbers of circumferential waves, that do not satisfy the relationship $k\times n$, have interaction only if their natural frequencies are very close to ratios 1:1, 1:2, 1:3 or other combinations with the frequency of the resonant mode. Only modes with an odd $m$ value of longitudinal half-waves can be considered for symmetry reasons [19,20] (if geometric imperfections with an even $m$ value are not introduced). In particular, asymmetric modes having up to three longitudinal half-waves ($M_1=3$, only odd $m$ values) and modes having $n$, $2\times n$, and $3\times n$ circumferential waves have been considered in the numerical calculations. For axisymmetric modes, up to $M_2=9$ has been used (only odd $m$ values).

### 2.3. Sanders–Koiter theory: geometric imperfections

Initial geometric imperfections of the circular cylindrical shell are considered only in radial direction. They are associated with zero initial stress. The radial imperfection $w_0$ is expanded in the same form of $w$, i.e. in a double Fourier series satisfying the boundary conditions (8a,c) at the shell edges

$$w_0(x,\theta)=\sum_{m=1}^{\tilde{M}_1}\sum_{n=1}^{\tilde{N}}\left[w^{(0)}_{m,n,c}\cos(n\theta)+w^{(0)}_{m,n,s}\sin(n\theta)\right]\sin(\lambda_m x)+\sum_{m=1}^{\tilde{M}_1}w^{(0)}_{m,0}\sin(\lambda_m x), \tag{10}$$

where $w^{(0)}_{m,n,c}$, $w^{(0)}_{m,n,s}$ and $w^{(0)}_{m,0}$ are the modal amplitudes of imperfections; $\tilde{N}$, $\tilde{M}_1$ and $\tilde{M}_2$ are integers indicating the number of terms in the expansion.

### 2.4. Sanders–Koiter theory: boundary conditions

Eqs. (8) give the boundary conditions for a simply supported shell. Eqs. (8a,c,e) are identically satisfied by the expansions of $u$, $v$, $w$ and $w_0$. Moreover, the continuity in $\theta$ of all the displacement is satisfied. As mentioned before Eq. (8d) is replaced with $N_x=0$; Eqs. (8b,d) are rewritten as follows [18] for $x=0$, $L$:

$$M_x=\frac{Eh^3}{12(1-\nu^2)}(k_x+\nu k_\theta)=0, \tag{11}$$

$$N_x=\frac{Eh}{1-\nu^2}(\varepsilon_{x,0}+\nu\varepsilon_{\theta,0})=0. \tag{12}$$

Eq. (11) is identically satisfied for the expressions of $k_x$ and $k_\theta$ given in Eqs. (2d,e).

Eq. (12) is not identically satisfied: according to Sanders–Koiter theory, see Eqs. (2a,b), and eliminating null terms at the shell edges, Eq. (12) can be rewritten as

$$\left[\frac{\partial\hat{u}}{\partial x}+\frac{1}{8}(1+\nu)\left(\frac{\partial v}{\partial x}-\frac{\partial u}{R\,\partial\theta}\right)^2+\frac{1}{2}\left(\frac{\partial w}{\partial x}\right)^2+\frac{\partial w}{\partial x}\frac{\partial w_0}{\partial x}\right]_{x=0,L}=0, \tag{13}$$

where $\hat{u}$ is a term added to the expansion of $u$, given in Eq. (9a), in order to satisfy exactly the axial boundary conditions $N_x=0$; its expression is reported in Appendix A.

It is worthwhile to stress that the present expansion does not satisfy the natural boundary condition (8d).

### 2.5. Fluid–structure interaction

The contained fluid is assumed to be incompressible and inviscid; these hypotheses turned out to be adequate for vibrations of water-filled shells [21]. The shell pre-stress due to the fluid weight is neglected; in the cases numerically investigated this pre-stress is extremely small. The nonlinear effects in the dynamic pressure and in the boundary conditions at the fluid–structure interface are also neglected. These nonlinear effects have been found to be negligible by Gonçalves and Batista [22] and Lakis and Laveau [23]; in fact, the amplitude of shell displacements remains small enough for linear fluid mechanics to be adequate.

In order to include the fluid effect in the Sanders–Koiter equations one should evaluate the energy contribution. Only kinetic energy $T_F$ is associated to inviscid still fluid; by using the Green's theorem, this is given by

$$T_F = \frac{1}{2}\rho_F \int_0^{2\pi}\int_0^L (\Phi)_{r=R}\dot{w}\,\mathrm{d}x\,R\,\mathrm{d}\theta, \tag{14}$$

where $\Phi$ is the velocity potential which is obtained in Appendix B.

### 2.6. Sanders–Koiter theory: Lagrange equations

The nonconservative damping forces are assumed to be of viscous type and are taken into account by using the Rayleigh's dissipation function

$$F = \frac{1}{2}\,c\int_0^{2\pi}\int_0^L (\dot{u}^2+\dot{v}^2+\dot{w}^2)\,\mathrm{d}x\,R\,\mathrm{d}\theta, \tag{15}$$

where $c$ has a different value for each term of the mode expansion. Simple calculations give

$$F = \frac{1}{2}(L/2)R\sum_{n=0}^{N}\sum_{m=1}^{M}\psi_n[c_{m,n,c}(\dot{u}^2_{m,n,c}+\dot{v}^2_{m,n,c}+\dot{w}^2_{m,n,c})+c_{m,n,s}(\dot{u}^2_{m,n,s}+\dot{v}^2_{m,n,s}+\dot{w}^2_{m,n,s})], \tag{16}$$

where

$$\psi_n = \begin{cases} 2\pi & \text{if } n=0,\\ \pi & \text{if } n>0. \end{cases} \tag{17}$$

The damping coefficient $c_{m,n,c\text{ or }s}$ is related to modal damping ratio, that can be evaluated from experiments, by $\zeta_{m,n,c\text{ or }s} = c_{m,n,c\text{ or }s}/(2\mu_{m,n}\omega_{m,n})$, where $\omega_{m,n}$ is the natural circular frequency of mode $(m, n)$ and $\mu_{m,n}$ is the modal mass of this mode, given by $\mu_{m,n} = \psi_n(\rho_S+\rho_V)h(L/2)R$, and the virtual mass due to contained fluid is

$$\rho_V = \frac{\rho_F}{\lambda_m h}\frac{I_n(\lambda_m R)}{I'_n(\lambda_m R)}. \tag{18}$$

The total kinetic energy of the system is

$$T = T_S + T_F. \tag{19}$$

The potential energy of the system is only the elastic strain energy of the shell

$$U = U_S. \tag{20}$$

In presence of axial loads acting on the shell, additional virtual work is done by the external forces. Let us consider a time-dependent axial load $\tilde{P}(t) = -P + P_D\cos\omega t$ (expressed in Newton) uniformly distributed on the shell ends; $\tilde{P}(t)$ is applied at both the shell ends; $\tilde{P}(t)$ is positive in the $x$ direction. In particular $-\tilde{P}(t)$ is applied at $x=0$ and $\tilde{P}(t)$ is applied at $x=L$. The axial distributed force $q_x$ has the following expression

$$q_x = \frac{\tilde{P}(t)}{2\pi R}[-\delta(x)+\delta(x-L)], \tag{21}$$

where $\delta$ is the Dirac function. The virtual work done by the axial load is

$$W = \int_0^{2\pi}\int_0^L \frac{\tilde{P}(t)}{2\pi R}[-\delta(x)+\delta(x-L)]u\,\mathrm{d}x R\,\mathrm{d}\theta = -2\tilde{P}(t)\sum_{m=1}^{M_{u2}} u_{m,0}(t). \tag{22}$$

The following notation is introduced for brevity

$$\mathbf{q} = \left\{u_{m,n,c}, u_{m,n,s}, v_{m,n,c}, v_{m,n,s}, w_{m,n,c}, w_{m,n,s}\right\}^{\mathrm{T}}. \tag{23}$$

The generic element of the time-dependent vector $\mathbf{q}$ is referred to as $q_j$; the dimension of $\mathbf{q}$ is dofs, which is the number of degrees of freedom used in the mode expansion.

The generalized forces $Q_j$ are obtained by differentiation of the Rayleigh's dissipation function and of the virtual work done by external forces

$$Q_j = -\frac{\partial F}{\partial \dot{q}_j} + \frac{\partial W}{\partial q_j} = -c_{m,n,i,j,c/s}\dot{q}_j + \begin{cases} 0 & \text{if } q_j = u_{m,n,c/s} \text{ with } n \neq 0,\ v_{m,n,c/s} \text{ or } w_{m,n,c/s}, \\ -2\tilde{P}(t) & \text{if } q_j = u_{m,0}, \end{cases} \tag{24}$$

where the subscript $c/s$ indicates $c$ or $s$. In numerical calculations $\tilde{f}$ will be set equal to zero and only axial excitation will be considered.

The Lagrange equations of motion for the fluid-filled shell are

$$\frac{\mathrm{d}}{\mathrm{d}t}\left(\frac{\partial T}{\partial \dot{q}_j}\right) - \frac{\partial T}{\partial q_j} + \frac{\partial U}{\partial q_j} = Q_j, \quad j = 1, \ldots, \text{dofs}, \tag{25}$$

where $\partial T/\partial q_j = 0$. These second-order equations have very long expressions containing quadratic and cubic nonlinear terms. In particular,

$$\frac{\mathrm{d}}{\mathrm{d}t}\left(\frac{\partial T}{\partial \dot{q}_j}\right) = \begin{cases} \rho_S h(L/2)\psi_n R\ddot{q}_j & \text{if } q_j = u_{m,n,c/s} \text{ or } v_{m,n,c/s}, \\ (\rho_S + \rho_v)h(L/2)\psi_n R\ddot{q}_j & \text{if } q_j = w_{m,n,c/s}, \end{cases} \tag{26}$$

which shows that no inertial coupling among the Lagrange equations exists for the shell with simply supported edges with the mode expansion used.

The very complicated term giving quadratic and cubic nonlinearities can be written in the form

$$\frac{\partial U}{\partial q_j} = \sum_{k=1}^{\text{dofs}} q_k f_{k,j} + \sum_{i,k=1}^{\text{dofs}} q_i q_k f_{i,k,j} + \sum_{i,k,l=1}^{\text{dofs}} q_i q_k q_l f_{i,k,l,j}, \tag{27}$$

where coefficients $f$ have long expressions that include also geometric imperfections.

## 3. Donnell's nonlinear shallow shell theory

A system of cylindrical coordinate is considered and $u$, $v$, $w$ are the longitudinal, circumferential and radial displacements respectively, but in this case $w$ is positive inwards; $w_0(x, \theta)$ is the geometric imperfection of the circular cylindrical shell associated with zero initial stress, is also taken positive inwards.

Considering the Donnell's nonlinear shallow shell theory, including geometric imperfections, the equation of motion is [21]

$$\begin{aligned} &D\nabla^4 w + ch\dot{w} + \rho_S h\ddot{w} - \frac{1}{R}\frac{\partial^2 F}{\partial x^2} \\ &\quad - \frac{1}{R^2}\left[\frac{\partial^2 F}{\partial \theta^2}\left(\frac{\partial^2 w}{\partial x^2} + \frac{\partial^2 w_0}{\partial x^2}\right) - 2\frac{\partial F}{\partial x \partial \theta}\left(\frac{\partial^2 w}{\partial x \partial \theta} + \frac{\partial^2 w_0}{\partial x \partial \theta}\right) + \frac{\partial^2 F}{\partial x^2}\left(\frac{\partial^2 w}{\partial \theta^2} + \frac{\partial^2 w_0}{\partial \theta^2}\right)\right] - f = 0, \end{aligned} \tag{28}$$

with the compatibility equation

$$\frac{\nabla^4 F}{Eh} + \frac{1}{R}\frac{\partial^2 w}{\partial x^2} + \frac{1}{R^2}\left[-\left(\frac{\partial w}{\partial x \partial \theta}\right)^2 - 2\frac{\partial^2 w}{\partial x \partial \theta}\frac{\partial^2 w_0}{\partial x \partial \theta} + \left(\frac{\partial^2 w}{\partial x^2} + \frac{\partial^2 w_0}{\partial x^2}\right)\frac{\partial^2 w}{\partial \theta^2} + \frac{\partial^2 w}{\partial x^2}\frac{\partial^2 w_0}{\partial \theta^2}\right] = 0, \tag{29}$$

where $D = Eh^3/[12(1-\nu^2)]$ is the flexural stiffness, $c$ the damping coefficient and $F$ is the in-plane stress function, $f$ is a distributed external load that is assumed equal to zero in the present study. In Eqs. (28) and (29) the biharmonic operator is defined as $\nabla^4 = [\partial^2/\partial x^2 + \partial^2/(R^2\partial\theta^2)]^2$. In the Donnell's nonlinear shallow shell theory the in-plane inertia is neglected. The forces per unit length in the axial and circumferential directions, as well as the shear force, are given in Refs. [24–27], see Appendix C for details.

### 3.1. Nonlinear Donnell's shallow shell theory: Galerkin expansion

The discretization procedure used in the present paper is fully explained in Ref. [10]; here a brief description is given; the shell radial displacement is expanded as

$$w(x,\theta,t)=\sum_{n=1}^{M_1}\sum_{m=1}^{N_1}[w_{m,n,c}(t)\cos(n\theta)+w_{m,n,s}(t)\sin(n\theta)]\sin(\lambda_m x)+\sum_{m=1}^{M}w_{2m-1,0}(t)\sin(\lambda_{2m-1}x), \tag{30}$$

where $\lambda_m = m\pi/L$, $m$ is the number of axial half-waves, $n$ is the number of circumferential waves, $t$ is the time, $w_{m,n,c}(t)$, $w_{m,n,s}(t)$, $w_{2m-1,0}(t)$ are the generalized coordinates, which are unknown functions of $t$.

The general expansion (30) is reduced to a 11 degrees of freedom (dof) model having: 6 asymmetric modes and 5 axisymmetric modes. The choice of this model is made after a deep convergence analysis of the static and dynamic behavior of the shell [10,14]. The fundamental mode of the shell analyzed in this work is $(1, n)$. In Ref. [14] the following expansion showed good accuracy:

$$\begin{aligned}w = {} & w_{1,n,c}(t)\sin(\eta)\cos(n\theta)+w_{1,n,s}(t)\sin(\eta)\sin(n\theta)+w_{3,n,c}(t)\sin(3\eta)\cos(n\theta)\\ & +w_{3,n,s}(t)\sin(3\eta)\sin(n\theta)+w_{1,2n,c}(t)\sin(\eta)\cos(2n\theta)+w_{1,2n,s}(t)\sin(\eta)\sin(2n\theta)\\ & +w_{1,0}(t)\sin(\eta)+w_{3,0}(t)\sin(3\eta)+w_{5,0}(t)\sin(5\eta)+w_{7,0}(t)\sin(7\eta)\\ & +w_{9,0}(t)\sin(9\eta),\end{aligned} \tag{31}$$

where $\eta = \pi x/L$ and $A_{m,n}(t)$, $B_{m,n}(t)$ and $A_{m,0}(t)$ are the generalized coordinates.

Geometric imperfections having the same shape of the modes included in the expansion of the radial displacement are introduced. In particular, the following "modal"' imperfections are considered:

$$w_0 = w^{(0)}_{1,n,c}\sin(\eta)\sin(n\theta)+w^{(0)}_{3,n,c}\sin(3\eta)\sin(n\theta)+w^{(0)}_{1,2n,c}\sin(\eta)\sin(2n\theta)+w^{(0)}_{1,0}\sin(\eta)+w^{(0)}_{3,0}\sin(3\eta), \tag{32}$$

where $w^{(0)}_{m,n,c}$ and $w^{(0)}_{m,0}$ are the modal imperfection amplitudes.

The expansion introduced for the radial displacement $w$ satisfies identically the boundary conditions and the continuity of the circumferential displacement $v$. The boundary conditions for the in-plane displacements are satisfied on the average [10,21]. When the expansion of $w$ and $w_0$ are substituted in the right-hand side of Eq. (28), a PDE for the stress function $F$ is obtained. The solution may be written as $F = F_h + F_p$ where $F_h$ is the homogeneous solution and $F_p$ is the particular solution [14]. See Appendix C for details.

Using Donnell's nonlinear shallow shell theory, the natural frequencies depending on the axial load [18,28] are given by

$$\omega^2_{m,n}(P)=\omega^2_{m,n,0}\left(1-\frac{P}{P_{\mathrm{cr}}}\right), \tag{33a}$$

$$\omega^2_{m,n,0}=\omega^2_{m,n}(P=0)=\frac{E}{R^2\rho_S}\left\{\frac{(m\pi R/L)^4}{((m\pi R/L)^2+n^2)^2}+\frac{(h/R)^2}{12(1-\nu^2)}\left[\left(\frac{m\pi R}{L}\right)^2+n^2\right]^2\right\}. \tag{33b}$$

## 4. Numerical results

In this section a benchmark problem, widely studied in the past [10,29,30], has been considered; this benchmark shell has the following characteristics: $h = 2\times10^{-3}$ m, $R = 0.2$ m, $L = 0.4$ m, $E = 2.1\times10^{11}$ N/m$^2$, $\nu = 0.3$, $\rho_S = 7850$ kg/m$^3$. For such a shell the classical buckling theory [17] predicts the following classical buckling load $P_{\mathrm{cl}} = 2\pi R\times2.54\times10^6$ N.

In using the Sanders–Koiter theory, several mode expansions have been considered, in order to perform a convergence analysis:

- Model A, 25 dof, does not include conjugate sine "modes" (only $u_{m,j,c}$, $v_{m,j,c}$ and $w_{m,j,c}$, are considered); in particular, the following modes are present: asymmetric modes $(1, n)$, $(1, 2n)$, $(3,n)$, $(3, 2n)$, $(1, 3n)$ for $u$, $v$ and $w$; axisymmetric modes (1, 0), (3, 0), (5, 0), (7, 0), (9, 0) for $u$ and $w$.

- Model B, 22 dof, does not include conjugate modes; in particular, the following modes are present: asymmetric modes (1, $n$), (1, 2$n$), (3, $n$) for $u$, and $w$ and (1, $n$), (1, 2$n$), (3, $n$), (3, 2$n$), (9, $n$), (1, 4$n$) for $v$; modes (1, 0), (3, 0), (5, 0), (7, 0), (9, 0) for $u$ and $w$.
- Model C, 30 dof, includes conjugate modes, ($u_{m,j,c}$, $u_{m,j,s}$), ($v_{m,j,c}$, $v_{m,j,s}$) and ($w_{m,j,c}$, $w_{m,j,s}$), are all considered. In particular, the following modes are present: asymmetric modes (1, $n$), (1, 2$n$), (3,$n$) for $u$, and $w$ and (1, $n$), (1, 2$n$), (3,$n$), (3, 2$n$) for $v$; axisymmetric modes (1, 0), (3, 0), (5, 0), (7, 0), (9, 0) for $u$ and $w$.
- Model D, 20 dof, the same of model C, but conjugate forms are not considered (only $u_{m,j,c}$, $v_{m,j,c}$ and $w_{m,j,c}$, are present).

Where not specified, results have been obtained with the Sanders–Koiter shell theory.

### 4.1. Static bifurcation

The first analysis is concerned with the static stability analysis of the compressed shell. When the perfect shell is compressed, it undergoes to a small amplitude axial-symmetric deformation, see e.g. Fig. 2, which has been obtained by using the linearized Donnell's shallow shell equations for $P/P_{cl} = 0.4$. The pre-buckling deformation of a perfect circular cylindrical shell is axisymmetric and the amplitude of asymmetric modes is zero, an edge effect is visible also. The buckling mode considered in the present analysis is (1, 5).

Increasing the axial load, the shell loses stability: using model $B$ one finds that beyond $P/P_{cl} = 0.947$ the shell loses stability; this load is the actual critical load, also called bifurcation load. Results presented in Fig. 3 have been obtained by means of the continuation software AUTO [15]. At the bifurcation point, $P/P_{cl} = 0.947$, two new solutions, bifurcated branches, are found; these branches are initially unstable and sub-critical, moreover the displacement field is given by asymmetric and axisymmetric modes. In order to follow these solutions, the axial load must be reduced up to the "folding" $P/P_{cl} = 0.311$. It should be noted that the upper branch presents an amplitude smaller than the lower branch; indeed, it is well known that circular cylindrical shells are stiffer outward than inward. In Fig. 3, dotted lines represent the solution obtained by Gonçalves and Del Prado [11]: they obtained bifurcation at $P/P_{cl} = 1$ because they neglected the pre-buckling effect; the post-critical behaviour is in good agreement, except for high amplitudes, in such case the theory used in Ref. [11] is less accurate. Pellicano and Amabili [10] obtained the buckling load using Donnell's nonlinear shallow shell theory at $P/P_{cl} = 0.95$ and folding at $P/P_{cl} = 0.2$. Using the model A, having more degrees of freedom, we obtain the critical load $P/P_{cl} = 0.949$ and the folding at $P/P_{cl} = 0.316$, i.e. almost the same results obtained with model B.

Such results show that even if the compression load is much smaller than the critical load, the shell could collapse; indeed, between $P = 30\%$ and 95% $P_{cl}$ there are three stable equilibrium positions and 2 unstable one. The "unperturbed" equilibrium position is represented by a small amplitude axial symmetric

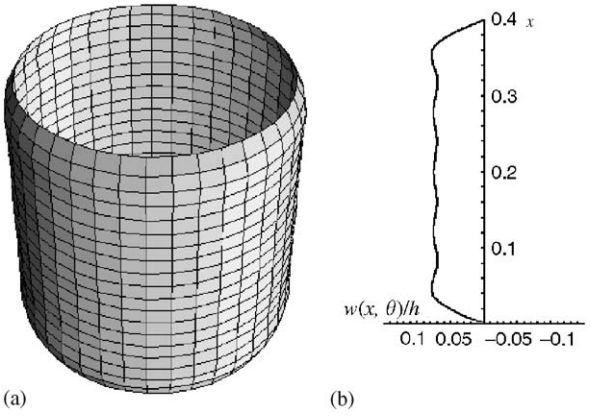


Fig. 2. Pre-buckling effect on a perfect shell: axial symmetric deformation; $P/P_{cl} = 0.4$. (a) 3D representation; (b) longitudinal section. Normalized amplitude with respect to the shell thickness $h$; Donnell's shallow shell theory.

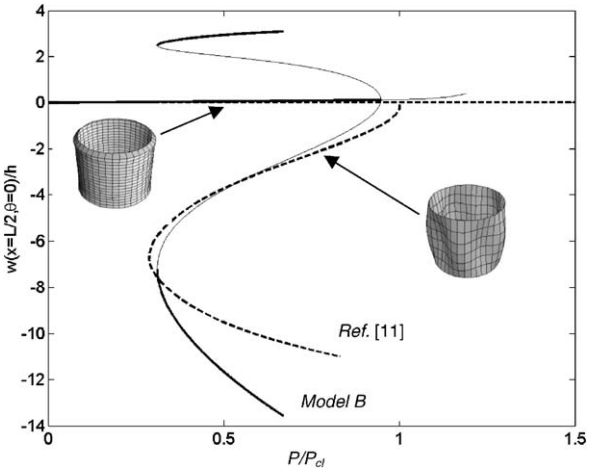


Fig. 3. Shell buckling: non-dimensional displacement of mid-point ($x = L/2$, $\theta = 0$). Comparison between Ref. [11] (– –) and the present theory, Model B, (—) stable solution, (—) unstable solution.

Table 1
Convergence test

| Modes eliminated from Model A | $P_{cr}/P_{cl}$ | $P_{fold}/P_{cl}$ |
|---|---|---|
| — | 0.9497 | 0.3158 |
| (1, 3n) | 0.9497 | 0.2993 |
| (3, 2n) | 0.9497 | 0.6075 |
| (3, n) | 0.9621 | 0.563 |
| (1, 3n) on $u$, $v$, $w$ and (3, 2n) on $u$, $w$ | 0.9496 | 0.3106 |

deformation; its basin of attraction is reduced as $P$ approaches $P_{cl}$ and a perturbation can cause a jump to one of the buckled positions, i.e. the collapse of the shell.

A convergence test is performed starting from the 25 dof model A; then, several modes are eliminated from the model A. In Table 1 results of the convergence test are summarized: mode (1, 3n), $n = 5$, can be eliminated without loss of accuracy; mode (3, n) cannot be eliminated; mode (3, 2n) can be eliminated from the expansion of $u$ and $w$ only. The result of such convergence analysis is that models C and D can be used without loss of accuracy.

Geometrical imperfections are considered in the static buckling behaviour presented in Fig. 4, where the bifurcation path is presented for several imperfection amplitudes. The imperfection is given on asymmetric mode (1,5) with positive value; the pitchfork bifurcation is immediately destroyed by the imperfection and is replaced by a folding (saddle node bifurcation); indeed, in Fig. 4 one can see that the imperfect shell exhibits a continuous deformation path. The picture is similar to that obtained in Ref. [10], but the amplitude is smaller because in this case we plot the outward deflection, positive part of Fig. 3; conversely in Ref. [10] the inward deflection was considered, obtained with the simpler Donnell's nonlinear shallow shell theory.

The effect of imperfections consists in a large reduction of the "critical load", which is identified by the folding point having the largest load (pre-buckling); the other folding is only slightly moved to the left hand by imperfections. In Table 2 the effect of asymmetric and axial symmetric imperfections is summarized.

### 4.2. Dynamic analysis: empty shell

In this section a periodic time varying axial load is considered; such kind of excitation gives rise to a direct excitation of the axisymmetric generalized coordinate $u_{m,0}$ according to Sanders–Koiter theory.

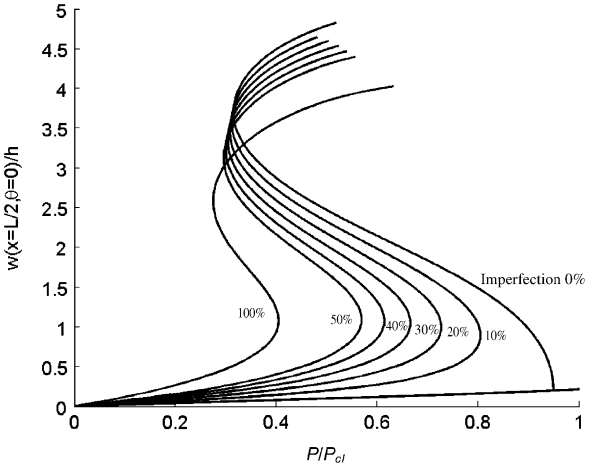


Fig. 4. Shell buckling: effect of geometric imperfections on mode $w^{(0)}_{1,5,c}$ (Model A). Imperfection amplitude: 100% $\equiv h$.

Table 2
Static buckling: effect of imperfections on modes (1,5) and (1,0). Results obtained with Sanders–Koiter theory if not differently specified

| $w^{(0)}_{1,5,c}/h$ | $w^{(0)}_{1,0}/h$ | $P_{cr}/P_{cl}$ | $P_{fold}/P_{cl}$ |
|---|---|---|---|
| 0 | 0 | 0.95 (Donnell) | 0.2 (Donnell) |
| 0 | 0 | 0.949 | 0.316 |
| 0.1 | 0 | 0.805 | 0.312 |
| 0.2 | 0 | 0.727 | 0.308 |
| 0.3 | 0 | 0.666 | 0.304 |
| 0.4 | 0 | 0.615 | 0.300 |
| 0.5 | 0 | 0.56 | 0.297 |
| 1 | 0 | 0.405 | 0.276 |
| 0 | 0.2 | 1.038 | 0.326 |
| 0 | 0.4 | 1.135 | 0.338 |

Here we are mainly interested to large amplitude of vibration due to period-doubling instability of asymmetric modes. When the excitation frequency is close to twice the linear frequency of a shell mode, a dynamic Mathieu-type instability can take place; the shell vibration is sub-harmonic and the amplitude can be quite large.

A first analysis is performed, using Model A, on a perfect shell by considering a purely harmonic axial load of increasing magnitude, i.e. no static preload is present: $\omega/\omega_{1,5(0)} = 1.9$ ($\omega_{1,5(0)} = 2\pi 484.22\,\text{rad/s}$ is the fundamental frequency of the shell without initial compression using Sanders theory and $\omega_{1,5(0)} = 2\pi 503.7\,\text{rad/s}$ using Donnell's shallow shell theory), $P = 0$, modal damping ratio $\zeta = 0.089$ on all modes; the dynamic axial load $P_D$ is increased starting from zero excitation up to the onset of instability. Periodic solutions, their stability and bifurcations are studied by means of continuation techniques [15]. When the amplitude of excitation is small, the shell vibrates axial symmetrically with small amplitude and the response is periodic; see Fig. 5. When $P_D/P_{cl} = 0.424$, a Period Doubling (PD) bifurcation is found; increasing the dynamic load the solution becomes unstable. From the bifurcation point a new solution takes place; it is slightly sub-critical and initially unstable. This response is no more axial symmetric, and both asymmetric and axisymmetric modes are excited. Note that an amplitude of oscillation of order of $h$ means the acceleration $a = \omega^2 h$ ($\omega = 2\pi 484.22\,\text{rad/s}$), which is about 1900 g!

In Fig. 5 a comparison among solutions obtained by Donnell's nonlinear shallow shell theory and model A (Sanders–Koiter) is shown; Donnell's nonlinear shallow shell theory underestimates the axial symmetric vibration; see Fig. 5(b). However, the bifurcation point is estimated very close to the Sanders–Koiter theory:

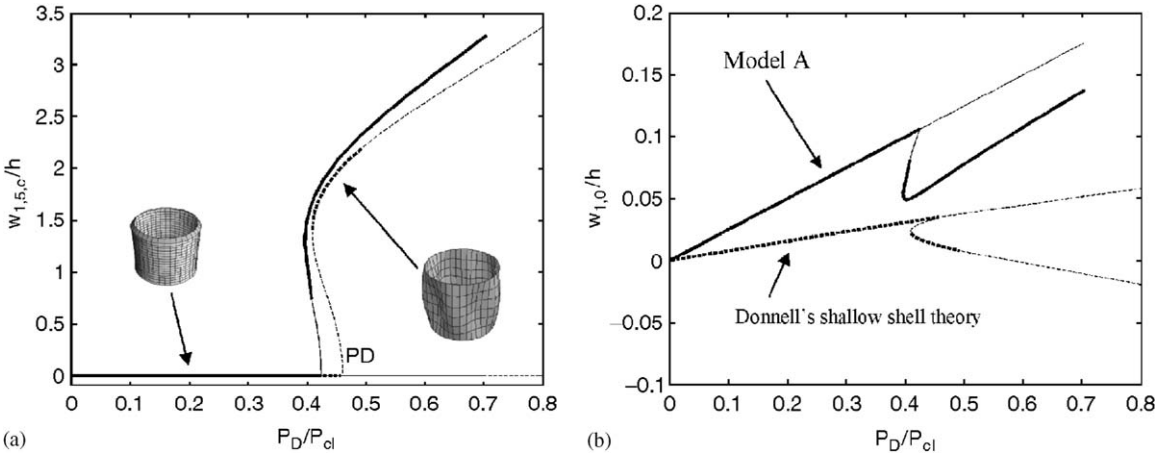


Fig. 5. Dynamic instability. "—" present analysis (Sanders–Koiter), "– –" Ref. [10] (Donnell's theory). Thick line: stable, thin line: unstable. (a) Amplitude of asymmetric mode (1,5); (b) axisymmetric mode (1,0); (PD) period-doubling bifurcation. $P = 0$, $\omega/\omega_{1,5(0)} = 1.9$, $\zeta = 0.089$.

Table 3
Dynamic critical load giving rise to period-doubling instability: present analysis (Sanders–Koiter, Model A); Refs. [10,13] (nonlinear Donnell's shallow shell theory); Ref. [13] (nonlinear Donnell's shallow shell theory with in-plane inertia). $P = 0$, $\zeta = 0.089$

| $\omega/\omega_{1,5(0)}$ | $P_{D\mathrm{cr}}/P_{\mathrm{cl}}$ Sanders–Koiter (present analysis, Model A) | $P_{D\mathrm{cr}}/P_{\mathrm{cl}}$ Donnell's nonlinear shallow shell [10] | $P_{D\mathrm{cr}}/P_{\mathrm{cl}}$ Donnell's nonlinear shallow shell [13] | $P_{D\mathrm{cr}}/P_{\mathrm{cl}}$ Donnell's nonlinear shallow shell [13] (with in-plane inertia) |
|---|---|---|---|---|
| 1.9 | 0.424 | 0.448 | 0.473 | 0.439 |
| 2 | 0.387 | 0.416 | 0.434 | 0.4 |

$P_D/P_{\mathrm{cl}} = 0.448$; the post-critical behaviour is in good agreement. The bifurcated branch obtained with Donnell's nonlinear shallow shell theory loses stability at $P_D/P_{\mathrm{cl}} = 0.49$, because of a bifurcation; from this point a new branch including the companion mode participation can take place. Such instability is not found using model A, because companion mode is not included.

A similar analysis is also performed for excitation frequency $\omega/\omega_{1,5(0)} = 2$; the smallest dynamic load, here called dynamic critical load $P_{D\mathrm{cr}}$, that gives rise to parametric instability is now $P_{D\mathrm{cr}}/P_{\mathrm{cl}} = 0.387$; also in this case Donnell's nonlinear shallow shell theory over-estimates the critical load ($P_{D\mathrm{cr}}/P_{\mathrm{cl}} = 0.416$), but the results are in good agreement.

Results about the critical dynamic load are summarized in Table 3; the Sanders–Koiter theory (present analysis) and the Donnell's nonlinear shallow shell theory [10,13] are compared. In Table 3 recent analyses, carried out by Jansen [13] using a reduced model, are presented; such results confirm the good quality of Donnell's theory. Moreover, such comparison confirms Jansen's comments: including in-plane inertia shows a moderate decrease of the dynamic critical load.

A further comparison is performed on a perfect shell by considering a small damping ratio $\zeta = 0.0008$ and a constant dynamic excitation amplitude $P_D/P_{\mathrm{cl}} = 0.01$; the excitation frequency is now varied. In Fig. 6 a comparison between Donnell's nonlinear shallow shell theory and the present theory (models A and D) is shown. When $\omega/\omega_{1,5}$ is close to 2, two PD bifurcations are found by all models, and a very good agreement is found. From the bifurcation points two 2T subharmonic branches (response having a period twice the excitation period) appear and the post-critical behaviour is now strongly sub-critical (softening); for higher amplitudes of oscillations Sanders–Koiter theory predicts a change in the response behaviour, which becomes hardening. This behaviour is not predicted by the less-accurate Donnell's nonlinear shallow shell theory. It

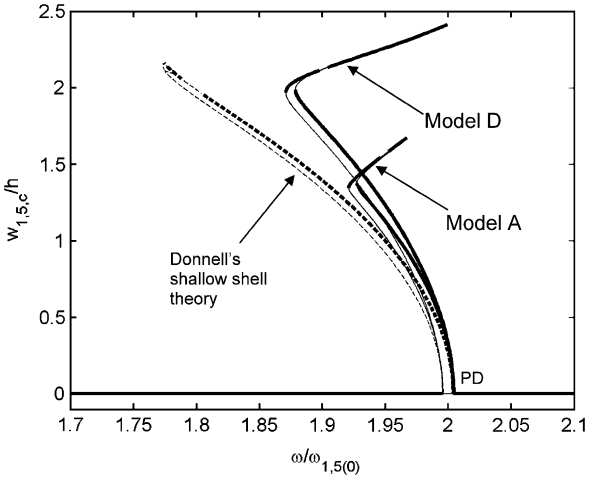


Fig. 6. Dynamic instability. "—" present analysis, "– –" Ref. [10]. Thick line stable solution; thin line unstable solution; (PD) period-doubling. $P = 0$, $P_D/P_{cl} = 0.01$, $\zeta = 0.0008$.

should be noted that model D does not agree properly with model A for high amplitudes of oscillation; this is due to the series truncation, which induces modelling errors in the nonlinear vibration.

The effect of geometric imperfections is now considered: $w^{(0)}_{1,5,c}/h = 0.1$, $w^{(0)}_{1,0}/h = 0.1$; the fundamental frequency is 484.22 Hz for the perfect shell and 479.82 Hz for the shell with such geometric imperfections; the principal parametric instability is found for $\omega/\omega_{1,5(0)} = 1.98181$ ($\omega_{1,5(0)}$ is the natural frequency of the perfect shell without preload), that means $\omega/\omega_{1,5} = 2$.

Simulations are performed using Model A with imperfections and $\omega/\omega_{1,5(0)} = 1.98181$, model A and Donnell's nonlinear shallow shell theory without imperfections and $\omega/\omega_{1,5(0)} = 2$ (in this case $\omega_{1,5(0)} = \omega_{1,5}$ because no imperfections nor static preload are present); the damping ratio is $\zeta = 0.0008$. In Fig. 7 the first asymmetric mode amplitude is represented versus the excitation amplitude. Before the bifurcation the amplitude is zero, but the shell is vibrating axial symmetrically, similarly to the case shown in Fig. 5; here, for the sake of brevity, the behaviour of axisymmetric modes is not reported. Donnell's nonlinear shallow shell theory predicts instability for $P_D/P_{cl} = 0.0038$, model A (perfect shell) find $P_D/P_{cl} = 0.0035$ and model A with imperfections find $P_D/P_{cl} = 0.0033$. Note that, with respect to Fig. 5, the ratio $P_D/P_{cl}$ is reduced about 100 times, due to the reduction of damping.

Such simulations show a good agreement among theories, i.e. the simpler Donnell's nonlinear shallow shell theory is sufficiently accurate, even though the in-plane inertia is neglected. Moreover, simulations show that the instability onset is not very sensitive to small geometric imperfections.

In Table 4 the effect of different geometric imperfections on the dynamic critical load $P_{Dcr}$ is summarized: the general comment is that geometric imperfections are not quite effective on the period-doubling instability; the only case where the influence is evident regards a relatively large imperfection (50% $h$) that gives rise to a large increase of the critical dynamic load, which is mainly due to axial symmetric outward imperfections, that make the shell much stiffer, as shown in the first column by large increase of the natural frequency. Note that no preload is present ($P = 0$) in all these cases.

In order to clarify the effect of asymmetric imperfection, model C, including the companion mode, is used. Only the imperfection on the fundamental mode is analyzed: the period-doubling instability seems to be insensitive to this kind of imperfection and the use of the largest model including conjugate modes does not change the behaviour, see Table 5.

Results presented in Tables 4 and 5 are obtained by means of a two-parameter continuation using the software AUTO, which allows for finding the minimum dynamic load versus the excitation frequency. Similar results have been obtained with a static preload $P/P_{cl} = 0.3$ and 0.6, with or without companion mode, but results are not presented here for the sake of brevity.

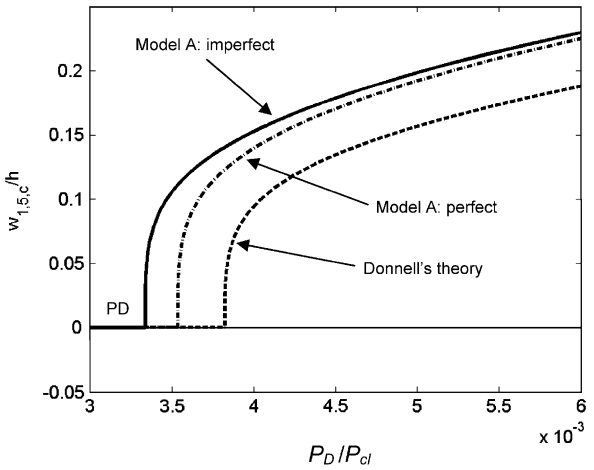


Fig. 7. Dynamic instability: model A, perfect (— · —) and imperfect (—) shell; Donnell's theory (— —). Imperfection amplitude: $w^{(0)}_{1,5,c}/h = w^{(0)}_{1,0}/h = w^{(0)}_{3,0}/h = 0.1$. (PD) Period doubling bifurcation; thick line 'stable'; thin line 'unstable'. $P = 0$, $\omega/\omega_{1,5} = 2$, $\zeta = 0.0008$.

Table 4
Dynamic buckling: effect of imperfections, model A (Sanders–Koiter); two-parameter continuation. $P = 0$, $\zeta = 0.0008$

| $\omega_{1,5}/\omega_{1,5(0)}$ | $w^{(0)}_{1,5,c}/h$ | $w^{(0)}_{1,15,c}/h$ | $w^{(0)}_{3,5,c}/h$ | $w^{(0)}_{1,0}/h$ | $w^{(0)}_{3,0}/h$ | $P_{D\mathrm{cr}}/P_{\mathrm{cl}}$ |
|---|---|---|---|---|---|---|
| 1 | 0 | 0 | 0 | 0 | 0 | 0.0038 (Donnell) |
| 1 | 0 | 0 | 0 | 0 | 0 | 0.0035 |
| 0.99091 | 0.1 | 0 | 0 | 0.1 | 0.1 | 0.0033 |
| 1.02912 | 0.1 | 0.1 | 0.1 | 0.1 | 0.1 | 0.0036 |
| 0.99975 | 0.1 | 0 | 0 | 0 | 0 | 0.0035 |
| 0.99117 | 0 | 0 | 0 | 0.1 | 0.1 | 0.0033 |
| 1.03715 | 0.1 | 0.1 | 0.1 | 0 | 0 | 0.0038 |
| 1.7001 | 0.5 | 0.5 | 0.5 | 0.5 | 0.5 | 0.0077 |
| 1.04611 | −0.1 | −0.1 | −0.1 | −0.1 | −0.1 | 0.004 |
| 1.00975 | 0 | 0 | 0 | −0.1 | −0.1 | 0.0037 |

In Fig. 8 the principal instability region is presented for $\zeta = 0.0008$ and $P/P_{\mathrm{cl}} = 0$: regions obtained with Donnell's nonlinear shallow shell and Sanders–Koiter theories are very close. Geometric imperfection ($w^{(0)}_{1,5,c}/h = 0.15$) gives a translation of the instability boundary, without changing the minimum value of $P_{D\mathrm{cr}}$.

A general conclusion is that small geometric imperfections, that give strong effects on the static buckling, are not effective on the parametric instability onset; Fig. 8. Similarly, the post-critical dynamic behaviour is not influenced by geometric imperfections; Fig. 7. Of course, the strong modification of the static post-critical path, should modify the dynamic properties; therefore the influence of initial imperfections on the post-critical dynamic behaviour and the escape from the potential well, in the case of high pre-compression, should be accurately investigated, such analysis is beyond the purposes of the present work.

### 4.3. Complex dynamics of empty shell with geometric imperfection

In this section the whole scenario of the shell dynamics is analyzed in the case of large axial preload, i.e. when the axial load is larger than the lower folding value, but lower than the critical value. In such case a jump to the buckled position is possible, and complex dynamics can take place. Geometric imperfection with $w^{(0)}_{1,5,c} = 0.15\,h$ is assumed.

Table 5
Dynamic buckling: effect of imperfections, model C (Sanders–Koiter, companion mode included); two-parameter continuation. $P = 0$, $\zeta = 0.0008$

| $\omega_{1,5(0)}$ | $w^{(0)}_{1,5,c}/h$ | $P_{D\mathrm{cr}}/P_{\mathrm{cl}}$ |
|---|---|---|
| 1 | 0 | 0.0035 |
| 0.99978 | 0.1 | 0.0036 |
| 0.99912 | 0.2 | 0.0036 |
| 0.99802 | 0.3 | 0.0036 |
| 0.99651 | 0.4 | 0.0037 |
| 0.99458 | 0.5 | 0.0037 |

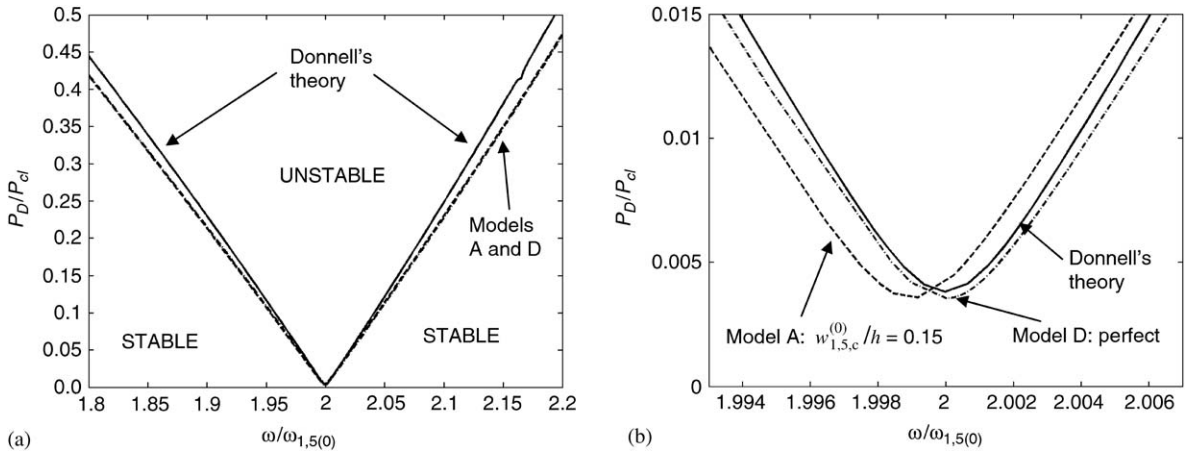


Fig. 8. Principal instability region: comparison of theories and effect of imperfections: (a) whole scenario; (b) enlarged view. $P = 0$, $\zeta = 0.0008$.

The bifurcation diagram is obtained by means of direct simulation using an adaptive step size Gear algorithm (Divpag of IMSL). The time history is sampled with the frequency of excitation in order to obtain Poincaré maps; the procedure is repeated by changing the control parameter, i.e. the excitation frequency, starting from $\omega/\omega_{1,5(0)} = 1.3$ and decreasing it up to 0.9. Each step of the bifurcation diagram is obtained after computing 2000 times the excitation period, in order to eliminate transient response, and recording 200 samples. It is to note that when a static preload is applied, the linear natural frequencies decrease as indicated by Eqs. (33a,b).

In Fig. 9 the bifurcation diagram is presented: a single line means periodic response; two points for each frequency indicate a 2T sub-harmonic response; more complex cases must be investigated deeply by analyzing 2D representations of Poincaré maps, time histories and spectra. By reducing the excitation frequency the period-doubling bifurcation is met for $\omega/\omega_{1,5(0)} = 1.235$; in the region $\omega/\omega_{1,5(0)} \in (1.121, 1.125)$ an amplitude modulation takes place. For $\omega/\omega_{1,5(0)} < 1.093$ there is a complex region where 2T periodic orbits, amplitude modulations and chaotic orbits are present; moreover, at $\omega/\omega_{1,5(0)} = 1.046$ a jump to the buckled position leads the shell to the collapse.

The chaotic dynamics appearing in the neighbourhood of $\omega/\omega_{1,5(0)} = 1.05$ is now analyzed in detail. A simulation is carried out by using data obtained from the bifurcation diagram as initial condition, in order to avoid the transient response (bifurcation diagrams are obtained after eliminating 2000 periods of excitation). In Fig. 10 time histories and spectra show that an irregular motion having a wide band spectrum is obtained. The spectral energy of asymmetric modes is mainly around $\Omega/\omega_{1,5(0)} = \omega/(\omega_{1,5(0)} \times 2)$ ($\Omega$ is the frequency variable in the Fourier domain), i.e. the response is mainly one half sub-harmonic. Conversely, the first

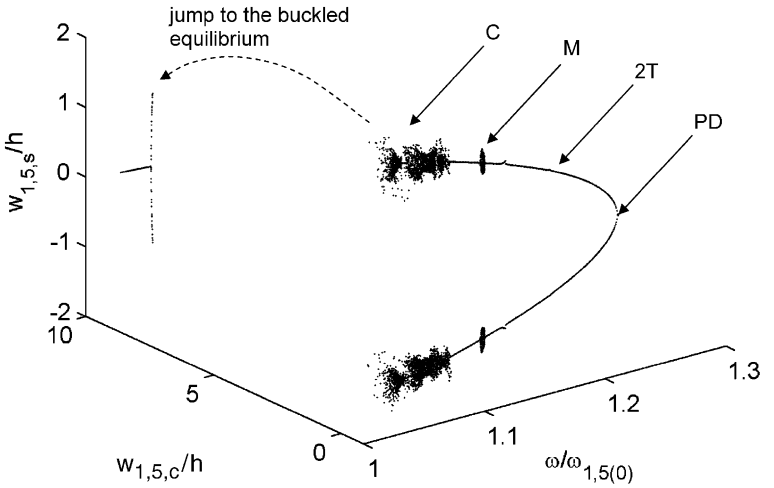


Fig. 9. Bifurcation diagrams (decreasing frequency), model C, $w^{(0)}_{1,5,c}/h = 0.15$, $P/P_{cl} = 0.6$, $P_D/P_{cl} = 0.04$, $\zeta = 0.0008$. 3D representation of the two conjugate modes (1,5). 'PD' period doubling bifurcation; '2T' one-half sub-harmonic response; 'M' amplitude modulation; 'C' chaotic response.

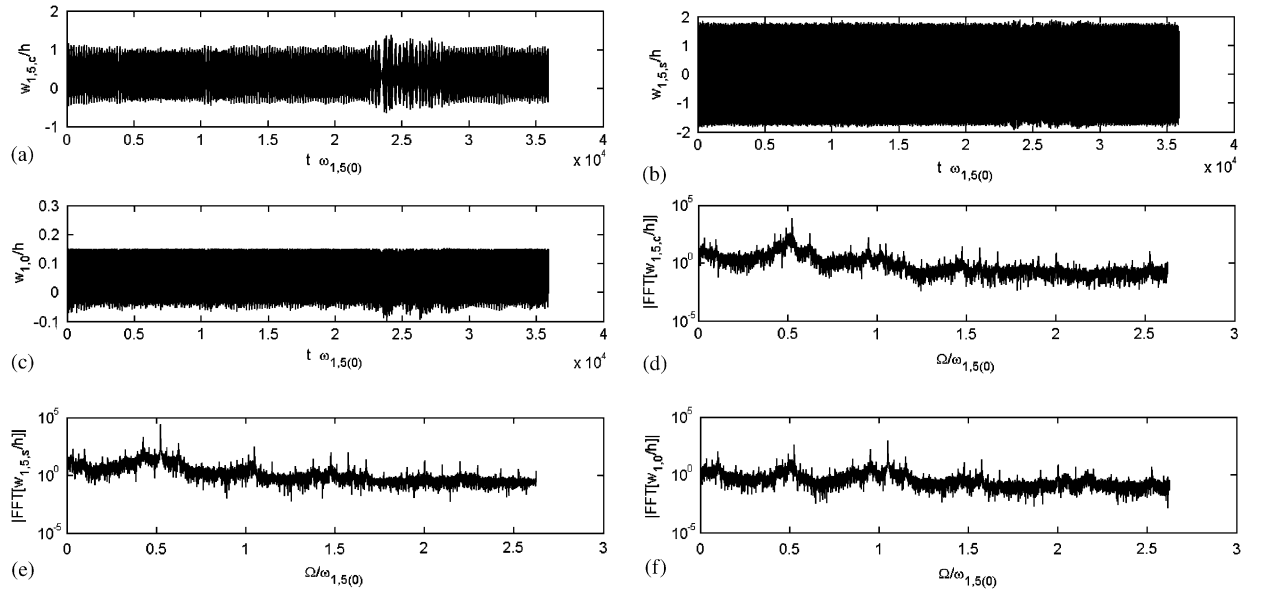


Fig. 10. System response, model C: $w^{(0)}_{1,5,c}/h = 0.15$, $P/P_{cl} = 0.6$, $P_D/P_{cl} = 0.04$, $\omega/\omega_{1,5(0)} = 1.05$, $\zeta = 0.0008$. (a) Time response of $w_{1,5,c}(t)/h$; (b) time response of $w_{1,5,s}(t)/h$; (c) time response of $w_{1,0}(t)/h$; (d) spectrum of $w_{1,5,c}(t)/h$; (e) spectrum of $w_{1,5,s}(t)/h$; (f) spectrum of $w_{1,0}(t)/h$.

axisymmetric mode has the main energy spectrum close to the excitation frequency. Poincaré maps, Fig. 11, confirm the chaotic character of the dynamics.

The chaotic regime has been investigated by using nonlinear time series techniques [16]. Starting from the modal response, the time history of the transversal displacement of a point in the middle of the shell is obtained, simulating an actual point measurement. The time history is sampled with sampling rate $\Delta t \times \omega_{1,5(0)} = 0.1995$. By analyzing the correlation function, a first minimum is found for $\tau = 15 \times \Delta t$; such time delay is used to create embedding coordinates [16]. Let us suppose that the time history $w(\hat{x}, \hat{\theta}, t)$ is

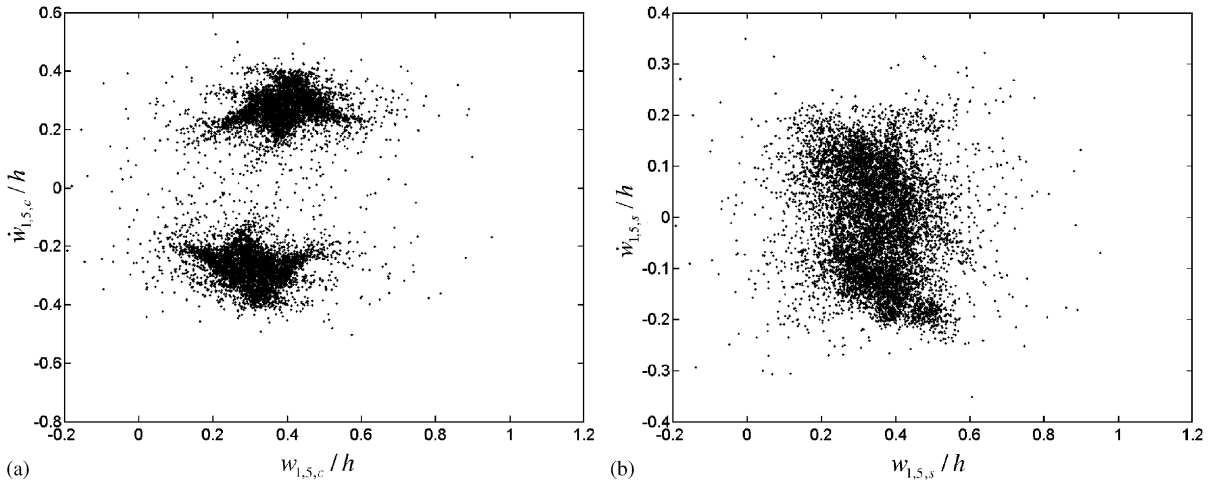


Fig. 11. Poincaré maps, model C, $w^{(0)}_{1,5,c}/h = 0.15$, $P/P_{\rm cl} = 0.6$, $P_D/P_{\rm cl} = 0.04$, $\omega/\omega_{1,5(0)} = 1.05$, $\zeta = 0.0008$. (a) Generalized coordinate $w_{1,5,c}$; (b) generalized coordinate $w_{1,5,s}$.

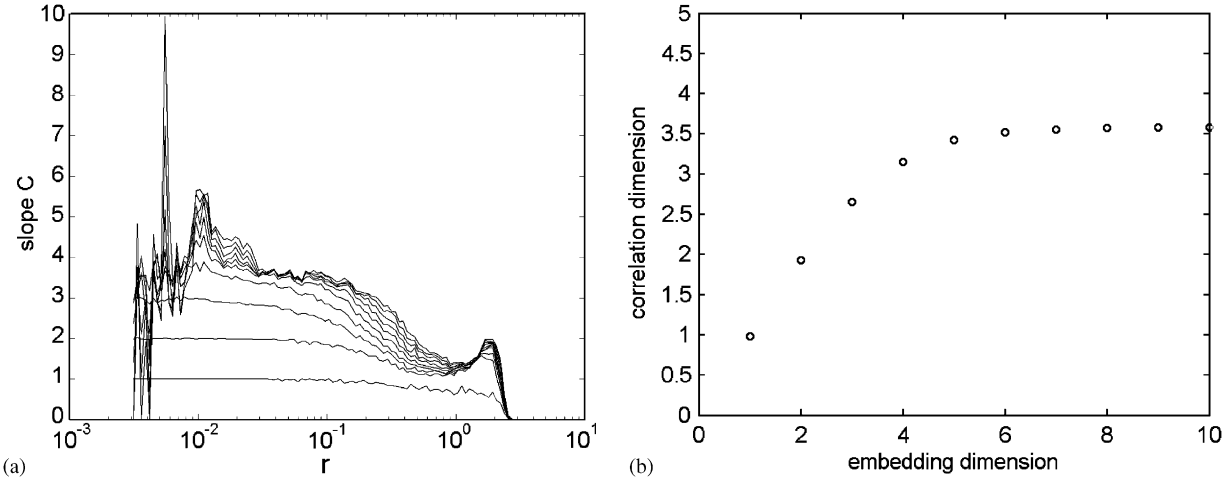


Fig. 12. Correlation dimension, model C, $w^{(0)}_{1,5,c}/h = 0.15$, $P/P_{\rm cl} = 0.6$, $P_D/P_{\rm cl} = 0.04$, $\omega/\omega_{1,5(0)} = 1.05$, $\zeta = 0.0008$. (a) Slope of the correlation integral versus the scale length; (b) correlation dimension versus the embedding dimension.

sampled, the time series is: $w_i = w(\hat{x}, \hat{\theta},\ i \times \Delta t)$, where $\Delta t$ is the sampling interval and $i = 1, \ldots, N_T$. A delay coordinate vector can be defined as follows: $\mathbf{v}_i = \{w_{i-(M-1)d}, w_{i-(M-2)d}, ..., w_i\}$, $i = (M-1) \times d, \ldots, N_T$; $d \times \Delta t$ is called time delay, and $M$ is the embedding dimension. The embedding theorem [30] states that if the time series consist of scalar measurements of a dynamical system and $M$ is large enough, then the time delay embedding provides a one-to-one image of the original phase space.

The Grassberger Procaccia [30,31] algorithm is applied to evaluate the correlation dimension from a time history of $10^5$ samples by using a Thailer window equal to $1500 \times \Delta t$ to eliminate spuriously correlated pairs. An estimation of the correlation dimension equal to 3.5 has been obtained, as shown in Fig. 12. This result shows that the dynamics is high dimensional and the attractor set is fractal, i.e. chaotic.

The maximum Lyapunov exponent is evaluated using an algorithm based on the work of Rosenstein et al. [32]. Basically the algorithm consists in considering two different but very close states of the system in the embedding space: $\mathbf{v}_{n'}$ and $\mathbf{v}_n$; the distance of these vectors is $\Delta_0 = \mathbf{v}_n - \mathbf{v}_{n'}$. Note that no matter how close are $\mathbf{v}_{n'}$

and $\mathbf{v}_n$ in time. Such distance can be thought as a small perturbation of an initial condition. Therefore one can follow the time evolution of the distance between two trajectories by writing: $\Delta_r = \mathbf{v}_{n+r} - \mathbf{v}_{n'+r}$; if $|\Delta_r| \approx |\Delta_0| e^{\lambda t}$ than $\lambda$ is the maximum Lyapunov exponent. Details of the algorithm used in the present paper can be found in Ref. [32]. From the time history analysis, the quantity $S = \lambda t$ is estimated versus: the time, the embedding dimension and the scale factor that is related to the initial distance. The slope of $S$ gives the maximum Lyapunov exponent with a good accuracy, if the analysis is repeated for several values of the perturbation and the embedding dimension. The maximum Lyapunov exponent is equal to $\Delta t \times 0.013$, see Fig. 13, which confirms the chaoticity of the response. Finally, using the algorithm developed in Ref. [33], the Lyapunov spectrum is estimated and two positive exponents are found. Moreover, the "Kaplan–Yorke" $K$–$Y$ dimension [34], which is strictly related to the correlation dimension, is estimated to be 3.7; such estimation is in agreement with the correlation dimension estimation.

The dimension $D_p$ of a phase space able to contain a certain attractor must be in the interval $[d_c] \leqslant D_p \leqslant 2 \times [d_c] + 1$, where $d_c$ is the correlation dimension and $[\cdot]$ means the greatest integer [35,36]. Therefore in our case $4 \leqslant D_p \leqslant 9$, i.e. 2 up to 4 dof could be necessary to reproduce such motion.

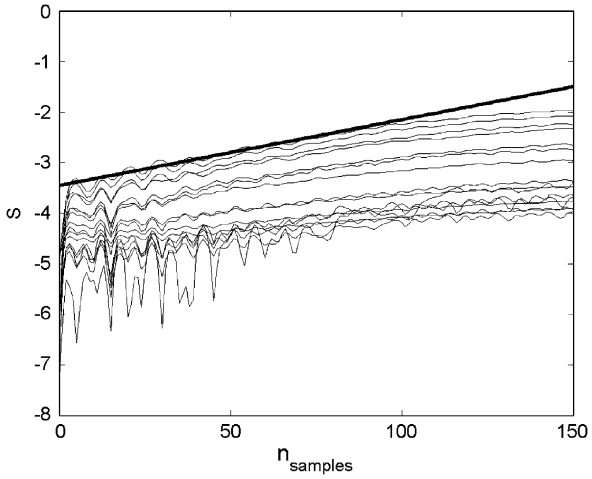


Fig. 13. Slope of maximum Lyapunov exponent, model C, $w^{(0)}_{1,5,c}/h = 0.15$, $P/P_{\mathrm{cl}} = 0.6$, $P_D/P_{\mathrm{cl}} = 0.04$, $\omega/\omega_{1,5(0)} = 1.05$, $\zeta = 0.0008$. Straight thick line: estimation of the actual slope.

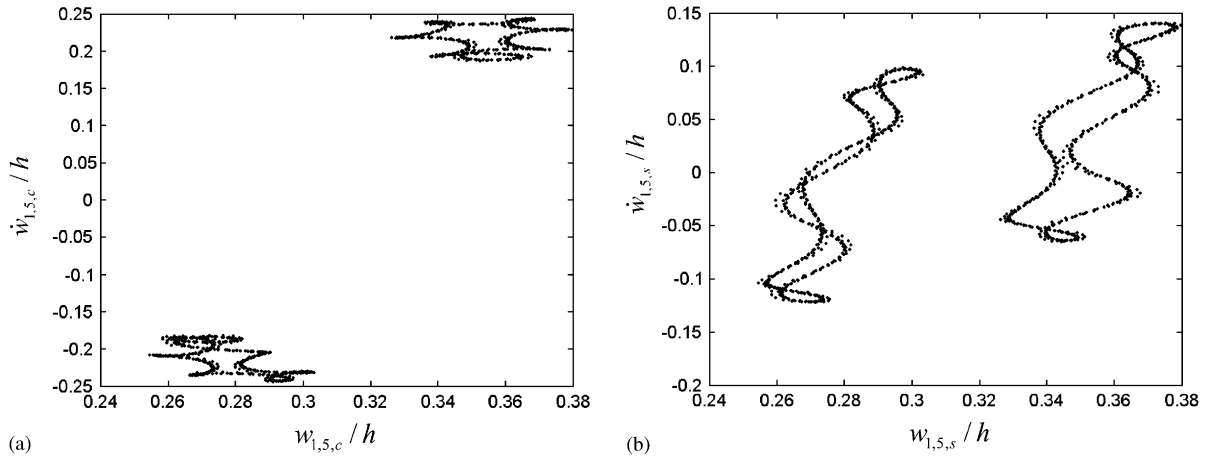


Fig. 14. Poincaré maps, model C, $w^{(0)}_{1,5,c}/h = 0.15$, $P/P_{\mathrm{cl}} = 0.6$, $P_D/P_{\mathrm{cl}} = 0.04$, $\omega/\omega_{1,5(0)} = 1.075$, $\zeta = 0.0008$. (a) Projection on the $(\dot{w}_{1,5,c}, w_{1,5,c})$-plane; (b) projection on the $(\dot{w}_{1,5,s}, w_{1,5,s})$-plane.

The previously mentioned time-series analyses allow to conclude that a high dimensional chaotic motion is found, where at least 4 modes participate to the dynamics: i.e. lower order model cannot be able to reproduce such chaotic response.

Close to the chaotic orbit for $\omega/\omega_{1,5(0)} = 1.075$ amplitude modulation motion is present. In Fig. 14 the Poincaré maps represent clearly such dynamics. Similarly, for $\omega/\omega_{1,5(0)} = 1.123$ amplitude modulation motion is found, see Fig. 15, even though the attractor is completely changed.

### 4.4. Dynamic analysis: water-filled shell

In this section a water-filled shell ($\rho_F = 1000\,\mathrm{kg/m^3}$) is considered. Similarly to the previous section, a periodic time varying axial load is applied.

A first analysis is carried out on the linear dynamics: the linear natural frequencies are evaluated by using both Sanders–Koiter theory (Model C) and Donnell's nonlinear shallow shell theory. The fundamental mode has 5 nodal diameters ($m = 1$, $n = 5$), similarly to the empty shell. The natural frequencies corresponding to modes used in the displacement expansion of model C (Sanders–Koiter theory) are compared with those obtained by Donnell's nonlinear shallow shell theory in Table 6: the maximum error is found for the fundamental mode (1,5), about 4%, and on the first axisymmetric mode (1,0), about 3%. Therefore, the linear behaviour of the shell is simulated with good accuracy by the Donnell's nonlinear shallow shell theory; also in the case of axisymmetric modes, for the specific test case, such theory does not give wrong results, even though it is well known in literature that such a theory should not be used for modes having $n<4$.

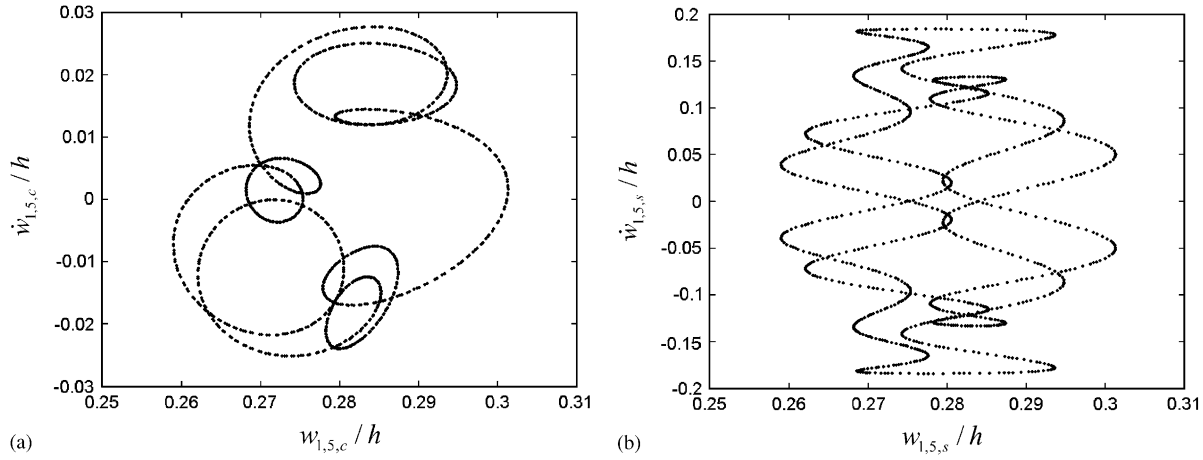


Fig. 15. Poincaré maps, model C, $w^{(0)}_{1,5,c}/h = 0.15$, $P/P_{\mathrm{cl}} = 0.6$, $P_D/P_{\mathrm{cl}} = 0.04$, $\omega/\omega_{1,5(0)} = 1.123$, $\zeta = 0.0008$. (a) Projection on the $(\dot{w}_{1,5,c}, w_{1,5,c})$-plane; (b) projection on the $(\dot{w}_{1,5,s}, w_{1,5,s})$-plane.

Table 6
Natural frequencies of the water-filled shell: comparison of theories

| Mode | Frequency (Hz) Sanders–Koiter | Frequency (Hz) Donnell's shallow shell | Error % |
|---|---|---|---|
| 1,5 | 260.75 | 271.26 | 4.03 |
| 1,10 | 838.75 | 851.55 | 1.53 |
| 3,5 | 1165.02 | 1185.09 | 1.72 |
| 1,0 | 1061.91 | 1091.26 | 2.76 |
| 3,0 | 2045.45 | 2049.77 | 0.21 |
| 5,0 | 2529.15 | 2531.03 | 0.07 |
| 7,0 | 2943.56 | 2944.68 | 0.04 |
| 9,0 | 3457.34 | 3458.12 | 0.02 |

Table 7
Critical dynamic buckling: effect of fluid and comparison theories. $P/P_{cl} = 0$, damping ratio 0.089

| $\omega/\omega_{1,5(0)}$ | $P_{Dcr}/P_{cl}$ (Sanders–Koiter) | $P_{Dcr}/P_{cl}$ (Donnell) | Presence of water |
|---|---|---|---|
| 2 | 0.704 | 0.722 | Yes |
| 2 | 0.387 | 0.416 | No |

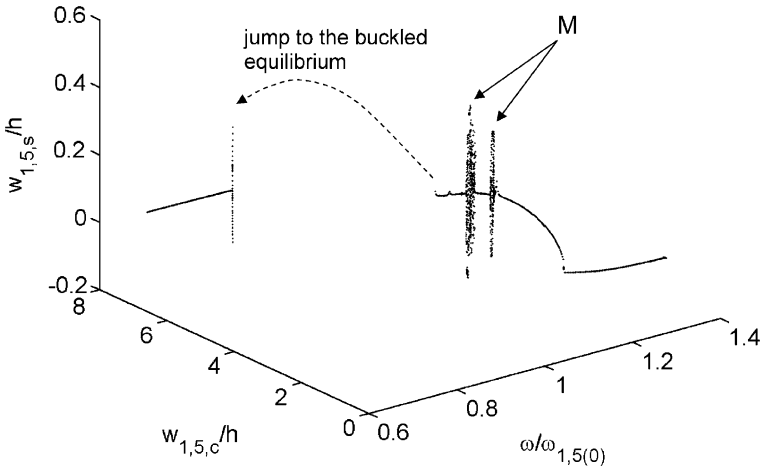


Fig. 16. Bifurcation diagrams, model C, water-filled shell, $w^{(0)}_{1,5,c}/h = 0.15$, $P/P_{cl} = 0.6$, $P_D/P_{cl} = 0.02$, $\zeta = 0.003$. 3D representation of the two conjugate modes (1,5). 'M' amplitude modulation.

A further comparison between Sanders–Koiter (Model C) and Donnell's nonlinear shallow shell theory is carried out in the case of axial excitation. A two-parameter continuation is performed in order to follow the dynamic instability bound (period-doubling bifurcation) when both frequency of excitation, $\omega$, and the amplitude of the sinusoidal excitation, $P_D$, are varied. The lowest value of $P_D$ which causes the parametric instability is found always at $\omega/\omega_{1,5(0)} = 2$; indeed, no pre-compression is exerted. Both Sanders–Koiter and Donnell's nonlinear shallow shell theories are in good agreement. In particular, both theories show that the presence of fluid induces an increase of the critical dynamic load, see Table 7. In the present analysis such safety effect is only due to the inertial effect of fluid; in fact, in the simulation the damping ratio was assumed to be the same with respect to the empty shell.

Generally, the presence of fluid results in a moderate increment of damping; therefore, in actual situations the dynamic critical load should increase even more.

In Fig. 16 the bifurcation diagram of the imperfect water-filled shell is presented for $w^{(0)}_{1,5,c}/h = 0.15$, $P/P_{cl} = 0.6$, $P_D/P_{cl} = 0.02$, damping ratio 0.3%: a single-value curve means periodic response. No chaotic regimes are found, only amplitude modulations take place for $\omega/\omega_{1,5(0)} \in (0.949, 0.962)$ and $\omega/\omega_{1,5(0)} \in (0.990, 0.997)$. Moreover, at $\omega/\omega_{1,5(0)} = 0.892$ a jump to the buckled position leads the shell to the collapse.

In order to investigate the amplitude modulation regime, a direct simulation has been performed for $\omega/\omega_{1,5(0)} = 0.955$. Fig. 17 shows the Poincaré map projected on a three-dimensional space ($w_{1,5,c}$, $w_{1,5,s}$, $w_{1,10,c}$); such modal coordinates have been selected after analyzing time histories and classical 2D Poincaré sections, e.g. ($\dot{w}_{i,j,c}$, $w_{i,j,c}$): 2D sections are meaningless because they do not clarify whether the attractor is one or two dimensional and the topology of the attractor. Therefore, several 3D projection have been carried out in order to find the best representation of the attractor. From Fig. 17 one can argue that the attractor set is one dimensional; however, it is wrapped up a 2D set that is topologically equivalent to a Torus. This means that such a dynamics is more complex than the classical amplitude modulations and at least 3 dof should be necessary to analyze such motion.

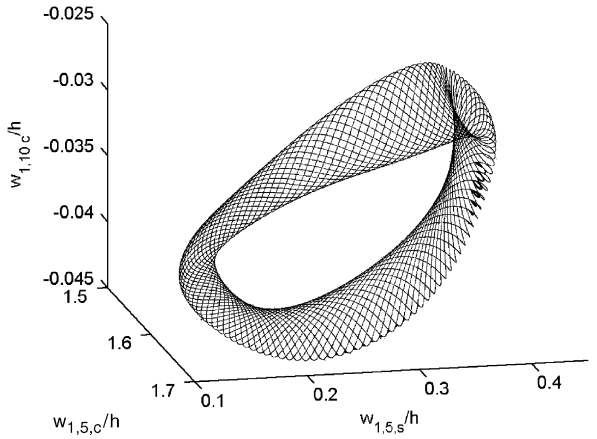


Fig. 17. Poincaré map, model C, water-filled shell, 3D representation. $w^{(0)}_{1,5,c}/h = 0.15$, $P/P_{\mathrm{cl}} = 0.6$, $P_D/P_{\mathrm{cl}} = 0.02$, $\omega/\omega_{1,5(0)} = 0.955$, $\zeta = 0.003$.

## 5. Conclusions

In the present paper, Sanders–Koiter shell theory has been applied in order to model the dynamics of the shell in presence of static and dynamic axial loads, geometric imperfections and fluid–structure interaction. A multimode approach have been developed in order to reduce the initial PPE problem to ODE, by using Lagrange equations. An accurate convergence test proved that the expansion used in the present work has been suitably truncated.

The accuracy of the widely used Donnell's nonlinear shallow shell theory have been tested, confirming that such approximate theory is sufficiently accurate. Comparisons with literature are provided. Comparisons among theories complete the investigation by Amabili [37] on nonlinear vibrations of shells under radial excitation, where different nonlinear shell theories were used and compared.

It is confirmed that the presence of a contained fluid gives safety effects on the instability onset, which appears through period-doubling bifurcation.

An accurate analysis of the effect of geometric imperfections on the dynamic instability onset and post-critical behaviour is carried out. The circular cylindrical shell under investigation was not particularly sensitive to small geometric imperfections, for which concern the instability onset.

The chaotic dynamics of pre-compressed shells is investigated in detail by means of nonlinear time-series techniques, extracting correlation dimension and Lyapunov exponents. The minimal dimension of the chaotic attractor has been evaluated through the K–Y dimension and correlation dimension estimators; results indicate that a strange attractor having dimension 3.5–3.7 appears, this means that such dynamical behaviour cannot be modelled by using low-dimensional models (e.g. 1 dof) the minimum number of dofs needed to obtain "certainly" such a dynamics is four [35].

## Acknowledgements

The authors thank MIUR (Italian Ministry of Education, University and Research), project PRIN-COFIN 2003, for supporting this research.

## Appendix A

### *A.1. In-plane boundary conditions*

Eqs. (8) give the boundary conditions for a simply supported shell; indeed in the present theory the axial load is included in the energy approach as virtual work. As a consequence that $\hat{u}$ is a second-order term in the shell displacement, it has not been inserted in the second-order terms that involve $u$ in Eq. (13).

All the generalized coordinates, except the six ones associated to the resonant mode ($m$, $n$), which are $u_{m,n,s}(t), v_{m,n,s}(t), w_{m,n,s}(t), u_{m,n,s}(t), v_{m,n,s}(t), w_{m,n,s}(t)$, are neglected because they are an infinitesimal of higher order. Calculations give [37]

$$\begin{aligned}\hat{u}(t) = & -\frac{1}{32}[a(t)+b(t)\cos(2n\theta)+c(t)\sin(2n\theta)]\sin(2m\pi x/L)-(m\pi/L)\\ & \times[w_{m,n,c}(t)\cos(n\theta)+w_{m,n,s}(t)\sin(n\theta)]\sum_{j=0}^{\tilde{N}}\sum_{i=1}^{\tilde{M}}\frac{i}{m+i}[A_{i,j}\cos(\mathrm{j}\theta)+B_{i,j}\sin(\mathrm{j}\theta)]\\ & \times\sin[(m+i)\pi x/L],\end{aligned} \tag{A.1}$$

where $\tilde{M}$ is the largest between $\tilde{M}_1$ and $\tilde{M}_2$ and

$$\begin{aligned}a(t) = & (4m\pi/L)(w_{m,n,c}^2+w_{m,n,s}^2)+(1+\nu)(m\pi/L)(v_{m,n,c}^2+v_{m,n,s}^2)\\ & +(1+\nu)[Ln^2/(m\pi R^2)](u_{m,n,c}^2+u_{m,n,s}^2)-2(1+\nu)(n/R)(v_{m,n,s}u_{m,n,s}-v_{m,n,c}u_{m,n,c}),\end{aligned} \tag{A.2}$$

$$\begin{aligned}b(t) = & (4m\pi/L)(w_{m,n,c}^2-w_{m,n,s}^2)+(1+\nu)(m\pi/L)(v_{m,n,s}^2-v_{m,n,c}^2)\\ & +(1+\nu)[Ln^2/(m\pi R^2)](u_{m,n,s}^2-u_{m,n,c}^2)-2(1+\nu)(n/R)(v_{m,n,s}u_{m,n,s}+v_{m,n,c}u_{m,n,c}),\end{aligned} \tag{A.3}$$

$$\begin{aligned}c(t) = & (8m\pi/L)w_{m,n,c}w_{m,n,s}+2(1+\nu)(m\pi/L)v_{m,n,c}v_{m,n,s}-2(1+\nu)[Ln^2/(m\pi R^2)]u_{m,n,c}u_{m,n,s}\\ & -2(1+\nu)(n/R)(v_{m,n,c}u_{m,n,s}-v_{m,n,s}u_{m,n,c}).\end{aligned} \tag{A.4}$$

## Appendix B

### *B.1. Fluid–structure interaction*

The fluid motion is described by the velocity potential $\Phi$, which satisfies the Laplace equation,

$$\nabla^2\Phi=\frac{\partial^2\Phi}{\partial x^2}+\frac{\partial^2\Phi}{\partial r^2}+\frac{1}{r}\frac{\partial\Phi}{\partial r}+\frac{1}{r^2}\frac{\partial^2\Phi}{\partial\theta^2}=0. \tag{B.1}$$

The fluid velocity vector $\mathbf{v}$ is related to $\Phi$ by $\mathbf{v}=-\nabla\Phi$. No cavitation is assumed at the fluid–shell interface,

$$\left(\frac{\partial\Phi}{\partial r}\right)_{r=R}=-\dot{w}. \tag{B.2}$$

Both ends of the fluid volume (in correspondence to the shell edges) are assumed to be open, so that a zero pressure is assumed there,

$$(\Phi)_{x=0}=(\Phi)_{x=L}=0. \tag{B.3}$$

A solution of Eq. (B.1) satisfying condition (B.3) is given by

$$\Phi=\sum_{m=1}^{\infty}\sum_{n=0}^{\infty}[\alpha_{mn}(t)\cos(n\theta)+\beta_{mn}(t)\sin(n\theta)][c_{mn}I_n(\lambda_m r)+d_{mn}K_n(\lambda_m r)]\sin(\lambda_m x), \tag{B.4}$$

where $I_n(r)$ and $K_n(r)$ are the modified Bessel functions of the first and second kind, respectively, of order $n$ and $\lambda_m=m\pi/L$. Eq. (B.4) must satisfy boundary condition (B.2) and $\Phi$ must be finite (regular) at $r=0$. By using the assumed mode expansion of $w$, given by Eq. (9c), the solution of the boundary value problem for internal fluid only is

$$\Phi=-\sum_{m=1}^{M}\sum_{n=0}^{N}[\dot{w}_{m,n,c}(t)\cos(n\theta)+\dot{w}_{m,n,s}(t)\sin(n\theta)]\frac{I_n(\lambda_m r)}{\lambda_m I_n'(\lambda_m R)}\sin(\lambda_m x), \tag{B.5}$$

where $I_n'(r)$ is the derivative of $I_n(r)$ with respect to its argument and $M$ is the largest between $M_{w1}$ and $M_{w2}$, which have been introduced in Eq. (9). Axisymmetric generalized coordinates are included with the subscript $c$

for brevity. Therefore, the dynamic pressure $p$ exerted by the contained fluid on the shell is given by

$$p = \rho_F(\dot{\Phi})_{r=R} = -\rho_F \sum_{m=1}^{M} \sum_{n=0}^{N} [\ddot{w}_{m,n,c}(t)\cos(n\theta) + \ddot{w}_{m,n,s}(t)\sin(n\theta)] \frac{I_n(\lambda_m R)}{\lambda_m I'_n(\lambda_m R)} \sin(\lambda_m x), \tag{B.6}$$

where $\rho_F$ is the mass density of the internal fluid. Eq. (B.6) shows that the fluid has an inertial effect on radial motion of the shell. In particular, the inertial effects are different for the asymmetric and the axisymmetric terms of the mode expansion. Hence, the fluid is expected to change the nonlinear behaviour of the fluid-filled shell. Usually the inertial effect of the fluid is larger for axisymmetric modes, thus enhancing the nonlinear behaviour of the shell.

## Appendix C

### C.1. Donnell's shallow shell theory: in-plane stresses and boundary conditions

$$N_x = \frac{1}{R^2}\frac{\partial^2 F}{\partial \theta^2}, \quad N_y = \frac{\partial^2 F}{\partial x^2}, \quad N_{x\theta} = -\frac{1}{R}\frac{\partial^2 F}{\partial x \partial \theta}. \tag{C.1}$$

The force–displacement relationships are [21]

$$(1-\nu^2)\frac{N_x}{Eh} = -\frac{\nu w}{R} + \frac{1}{2}\left(\frac{\partial w}{\partial x}\right)^2 + \frac{\partial w}{\partial x}\frac{\partial w_0}{\partial x} + \frac{\nu}{2}\left(\frac{\partial w}{R\partial \theta}\right)^2 + \nu\frac{\partial w}{R\partial\theta}\frac{\partial w_0}{R\partial\theta} + \frac{\partial u}{\partial x} + \frac{\nu}{R}\frac{\partial v}{\partial \theta}, \tag{C.2}$$

$$(1-\nu^2)\frac{N_\theta}{Eh} = -\frac{w}{R} + \frac{\nu}{2}\left(\frac{\partial w}{\partial x}\right)^2 + \nu\frac{\partial w}{\partial x}\frac{\partial w_0}{\partial x} + \frac{1}{2}\left(\frac{\partial w}{R\partial \theta}\right)^2 + \frac{\partial w}{R\partial\theta}\frac{\partial w_0}{R\partial\theta} + \nu\frac{\partial u}{\partial x} + \frac{1}{R}\frac{\partial v}{\partial \theta}, \tag{C.3}$$

$$(1-\nu^2)\frac{N_{x\theta}}{Eh} = 2(1-\nu)\left[\frac{1}{R}\frac{\partial w}{\partial x}\frac{\partial w}{\partial \theta} + \frac{1}{R}\frac{\partial w}{\partial x}\frac{\partial w_0}{\partial \theta} + \frac{1}{R}\frac{\partial w_0}{\partial x}\frac{\partial w}{\partial \theta} + \frac{1}{R}\frac{\partial u}{\partial \theta} + \frac{\partial v}{\partial x}\right]. \tag{C.4}$$

Considering a simply supported shell, the boundary conditions are

$$w = w_0 = 0 \quad \text{for } x = 0, L, \tag{C.5}$$

$$M_x = -D\left[\frac{\partial^2 w}{\partial x^2} + \nu\left(\frac{\partial^2 w}{R^2\partial\theta^2}\right)\right] = 0 \quad \text{for } x = 0, L, \tag{C.6}$$

$$\frac{\partial^2 w_0}{\partial x^2} = 0, \quad N_x = \tilde{N}_x(t) \quad \text{and} \quad v = 0 \quad \text{for } x = 0, L. \tag{C.7}$$

The external axial load is given by a constant compressive load $-P$ (expressed in Newton) and a sinusoidal time varying excitation having amplitude $P_D$ and angular frequency $\omega$

$$\tilde{N}_x(t) = -\frac{P}{2\pi R} + \frac{P_D}{2\pi R}\cos\omega t, \tag{C.8}$$

where $\tilde{N}_x(t)$ is a force per unit length [N/m].

The boundary conditions in Eqs. (C.5, C.6) are exactly satisfied by the expansion of the transversal displacement $w$; such expansion respects exactly the continuity of circumferential displacement [10]:

$$\int_0^{2\pi} \frac{\partial v}{\partial \theta}\,\mathrm{d}\theta = \int_0^{2\pi}\left[\frac{1}{Eh}\left(\frac{\partial^2 F}{\partial x^2} - \nu\frac{\partial^2 F}{R^2\partial\theta^2}\right) + \frac{w}{R} - \frac{1}{2}\left(\frac{\partial w}{R\partial\theta}\right)^2\right]\mathrm{d}\theta = 0. \tag{C.9}$$

The homogeneous part of the stress function satisfies the in-plane boundary conditions, Eq. (C.7), on the average

$$\int_0^{2\pi} N_x R\,\mathrm{d}\theta = 2\pi R\tilde{N}_x(t), \tag{C.10a}$$

$$\int_0^{2\pi}\int_0^{L} N_{x\theta}R\,\mathrm{d}x\,\mathrm{d}\theta = 0. \tag{C.10b}$$

Once the stress function is obtained, the classical Galerkin procedure is followed to project the governing equation into the base considered. A nonlinear system of coupled differential equations is obtained.

## References


[1] C.D. Babcock, Shell stability, *Journal of Applied Mechanics* 50 (1983) 935–940.
[2] C.R. Calladine, Understanding imperfection-sensitivity in the buckling of thin-walled shells, *Thin-Walled Structures* 23 (1995) 215–235.
[3] J.G. Teng, Buckling of thin shells: recent advances and trends, *Applied Mechanics Reviews* 49 (4) (1996) 263–274.
[4] M. Amabili, M.P. Païdoussis, Review of studies on geometrically nonlinear vibrations and dynamics of circular cylindrical shells and panels, with and without fluid–structure interaction, *Applied Mechanics Reviews* 56 (2003) 349–381.
[5] J.C. Yao, Dynamic stability of cylindrical shells under static and periodic axial and radial load, *AIAA Journal* 1 (6) (1963) 457–468.
[6] A. Vijayaraghavan, R.M. Evan-Iwanowski, Parametric instability of circular cylindrical shells, *Journal of Applied Mechanics* 34 (1967) 985–990.
[7] A.A. Bondarenko, P.I. Galaka, Parametric instability of Glass-plastic cylindrical shells, *Soviet Applied Mechanics* 13 (1977) 411–414.
[8] K. Nagai, N. Yamaki, Dynamic stability of circular cylindrical shells under periodic compressive forces, *Journal of Sound and Vibration* 59 (3) (1978) 425–441.
[9] V.D. Kubenko, P.S. Koval'chuk, Nonlinear problems of the vibration of thin shells (review), *International Applied Mechanics* 34 (1998) 703–728.
[10] F. Pellicano, M. Amabili, Stability and vibration of empty and fluid-filled circular cylindrical shells under static and periodic axial loads, *International Journal of Solids and Structures* 40 (2003) 3229–3251.
[11] P.B. Gonçalves, ZJGN Del Prado, Nonlinear oscillations and stability of parametrically excited cylindrical shells, *Meccanica* 37 (2002) 569–597.
[12] A.A. Popov, Parametric resonance in cylindrical shells: a case study in the nonlinear vibration of structural shells, *Engineering Structures* 25 (2003) 789–799.
[13] E. Jansen, Dynamic stability problems of anisotropic cylindrical shells via a simplified analysis, *Nonlinear Dynamics* 39 (2005) 349–367.
[14] G. Catellani, F. Pellicano, D. Dall'Asta, M. Amabili, Parametric instability of a circular cylindrical shell with geometric imperfections, *Computers & Structures* 82 (2004) 2635–2645.
[15] E.J. Doedel, A.R. Champneys, T.F. Fairgrieve, Y.A. Kuznetsov, B. Sandstede, X. Wang, *AUTO 97: Continuation and Bifurcation Software for Ordinary Differential Equations (with HomCont)*, Concordia University, Montreal, Canada, 1998.
[16] H. Kantz, T. Schreiber, *Nonlinear Time Series Analysis*, Cambridge University Press, Cambridge, 1997.
[17] N. Yamaki, *Elastic Stability of Circular Cylindrical Shells*, North-Holland, Amsterdam, 1984.
[18] A.W. Leissa, *Vibration of Shells*, *NASA SP-288*, Government Printing Office, Washington, DC, now available from The Acoustical Society of America, 1993.
[19] M. Amabili, F. Pellicano, M.P. Païdoussis, Non-linear dynamics and stability of circular cylindrical shells containing flowing fluid—part II: large-amplitude vibrations without flow, *Journal of Sound and Vibration* 228 (1999) 1103–1124.
[20] M. Amabili, F. Pellicano, M.P. Païdoussis, Non-linear dynamics and stability of circular cylindrical shells containing flowing fluid—part III: truncation effect without flow and experiments, *Journal of Sound and Vibration* 237 (2000) 617–640.
[21] M. Amabili, Theory and experiments for large-amplitude vibrations of empty and fluid-filled circular cylindrical shells with imperfections, *Journal of Sound and Vibration* 262 (2003) 921–975.
[22] P.B. Gonçalves, R.C. Batista, Non-linear vibration analysis of fluid-filled cylindrical shells, *Journal of Sound and Vibration* 127 (1988) 133–143.
[23] A.A. Lakis, A. Laveau, Non-linear dynamic analysis of anisotropic cylindrical shells containing a flowing fluid, *International Journal of Solids and Structures* 28 (1991) 1079–1094.
[24] H.-N. Chu, Influence of large amplitudes on flexural vibrations of a thin circular cylindrical shell, *Journal of Aerospace Science* 28 (1961) 602–609.
[25] DA. Evensen, *Nonlinear Flexural Vibrations of Thin-Walled Circular Cylinders*, *NASA TN D-4090*, Government Printing Office, Washington, DC, 1967.
[26] J.C. Chen, C.D. Babcock, Nonlinear vibrations of cylindrical shells, *AIAA Journal* 13 (1975) 868–876.
[27] M. Amabili, F. Pellicano, M.P. Païdoussis, Non-linear dynamics and stability of circular cylindrical shells containing flowing fluid—part I: stability, *Journal of Sound and Vibration* 225 (1999) 655–699.
[28] W. Soedel, *Vibrations of Shells and Plates*, Marcel Dekker Inc., New York, 1993.
[29] A.A. Popov, J.M.T. Thompson, F.A. McRobie, Low dimensional models of shell vibrations. Parametrically excited vibrations of cylindrical shells, *Journal of Sound and Vibration* 209 (1998) 163–186.
[30] P. Grassberger, I. Procaccia, Measuring the strangeness of strange attractors, *Physica D* 9 (1983) 189–208.
[31] P. Grassberger, I. Procaccia, Characterization of strange attractors, *Physical Review Letters* 50 (1983) 346–349.

[32] M.T. Rosenstein, J.J. Collins, C.J. De Luca, A practical method for calculating largest Lyapunov exponents from small data sets, *Physica D* 65 (1993) 117.
[33] M. Sano, Y. Sawada, Measurement of the Lyapunov spectrum from a chaotic time series, *Physical Review Letters* 55 (1985) 1082–1085.
[34] J. Kaplan, J. Yorke, Chaotic behavior of multidimensional difference equations, in: H.O. Peitgen, H.O. Walther (Eds.), *Functional Differential Equations and Approximation of Fixed Points*, Springer, New York, 1987.
[35] R. Mañé, On the dimension of compact invariant sets of certain non-linear maps, in: Rand, Young (Eds.), *Dynamical Systems and Turbulence*, Springer Lecture Notes in Mathematics, Vol. 898, 1981, Springer, New York, pp. 230–242.
[36] J.-P. Eckmann, D. Ruelle, Ergodic theory of chaos and strange attractors, *Reviews of Modern Physics* 57 (3) (1985) 617–656.
[37] M. Amabili, Comparison of shell theories for large-amplitude vibrations of circular cylindrical shells: Lagrangian approach, *Journal of Sound and Vibration* 264 (2003) 1091–1125.